SYNTHESIS OF MAGNETIC OXIDE NANOPARTICLES USING MICROEMULSIONS

By

VINOD KUMAR PILLAI

A DISSERTATION PRESENTED TO THE GRADUATE SCHOOL
OF THE UNIVERSITY OF FLORIDA IN PARTIAL FULFILLMENT
OF THE REQUIREMENTS FOR THE DEGREE OF
DOCTOR OF PHILOSOPHY

UNIVERSITY OF FLORIDA

1995

To

My Parents

ACKNOWLEDGMENTS

I would like to express my sincere appreciation to Professor Dinesh O. Shah, chairman of my supervisory committee, for his guidance and encouragement during my Ph.D. program. I would also like to thank Professors Brij M. Moudgil, R. Narayanan, Gerald B. Westermann-Clark, Chang W. Park, Larry Hench and Gar Hoflund for their valuable time and advice as members of my Ph.D. supervisory committee.

I wish to thank all my friends and colleagues at the Department of Chemical Engineering for all their help and support. I thank Drs. Promod Kumar, C. P. Singh, S. G. Oh, Y. K. Rao and Ken Miller, who helped me when I first joined our research group, Dr. Hingorani and Sandra, and the present group, Julie, Jennifer, Nancy, Alex, Manish, Paul, Peter, Sarv and Steve, for making it such a pleasant experience for me to come to the lab everyday; I will always remember all the fun we had (and all the work we did) as a group. I wish all of them the best of luck in future endeavors. I would also like to acknowledge the Major Analytical Instrumentation Center for their help with electron microscopy and x-ray diffraction, and the National Science Foundation for their financial support.

Finally, I would like to thank my parents, my brother Satish, and my sister Renuka for all their love and encouragement over the past five years.

TABLE OF CONTENTS

ACKNOWLEDGMENTS iii

LIST OF TABLES vii

LIST OF FIGURES viii

Abstract x

CHAPTERS

1 INTRODUCTION 1
1.1 Importance of Nanoparticles 1
1.2 Synthesis of Nanoparticles 2
1.3 Nanoparticles for Magnetic Recording 5
1.3.1 Requirements of Particulate Recording Media 6
1.3.1.1 Retentivity 6
1.3.1.2 Coercivity 7
1.3.1.3 Switching field distribution 7
1.3.1.4 Anisotropy 8
1.3.1.5 Particle Size 9
1.4 Thesis Organization 10

2 MICROEMULSIONS AND SYNTHESIS OF NANOPARTICLES 12
2.1 Introduction 12
2.2 Microstructure of Microemulsions 14
2.3 Phase Behavior and Solubilization in Microemulsions 17
2.4 Thermodynamic Stability of Microemulsions 19
2.5 Dynamic Structure and Reactions in Microemulsions 25
2.6 Particle Synthesis in Microemulsions 31

3 MICROEMULSION CHARACTERIZATION 34
3.1 Introduction 34
3.2 Theoretical Aspects of Solubilization 34
3.2.1 Curvature Effect in Microemulsions 36
3.2.2 Attractive Interaction between Microemulsion Droplets ... 38

3.2.3 Solubilization Capacity in Microemulsions 40
3.3 Experimental Procedure 40
3.3.1 Materials 41
3.3.2 Methods 42
3.4 Results and Discussion 42

4 SYNTHESIS OF IRON OXIDE USING MICROEMULSIONS 50
4.1 Introduction 50
4.2 Synthesis of γ-Fe_2O_3 52
4.2.1 Experimental Procedure 52
4.2.1.1 Materials 52
4.2.2.2 Methods 52
4.2.2 Results and Discussion 56
4.3 Synthesis of Cobalt modified Iron Oxide 61
4.3.1 Experimental Procedure 64
4.3.2 Results and Discussion 64
4.4 Conclusions 67

5 SYNTHESIS OF BARIUM FERRITE USING MICROEMULSIONS .. 68
5.1 Introduction 68
5.2 Experimental Procedure 70
5.2.1 Materials 70
5.2.2 Methods 71
5.3 Results and Discussion 75
5.4 Conclusions 84

6 REACTION KINETICS IN MICROEMULSIONS 85
6.1 Introduction 85
6.2 Experimental Procedure 89
6.2.1 Materials 89
6.2.2 Methods 89
6.3 Results and Discussion 91
6.4 Conclusions 103

7 CONCLUSIONS AND RECOMMENDATIONS FOR FUTURE WORK 105
7.1 Conclusions 105
7.2 Cost Analysis and Recycle 107
7.3 Recommendations for Future Work 110

REFERENCE LIST 112

BIOGRAPHICAL SKETCH 128

LIST OF TABLES

Table		page
4.1	Composition of the microemulsion systems used for the synthesis reactions	53
4.2	Comparison of magnetic properties for iron oxide and cobalt doped iron oxide nanoparticles	67
5.1	Composition of the microemulsion systems used for the synthesis reactions	71
5.2	Magnetic Properties of microemulsion derived barium ferrite	82
6.1	Compositions of microemulsion systems used for studying effects of alcohol and oil chain length	91
7.1	Cost analysis for the preparation of 1 gm of barium ferrite using microemulsions	108

LIST OF FIGURES

Figure		page
1.1	Hysteresis loop (plot of magnetization versus applied field) for a typical recording medium	8
2.1	Idealized ternary phase diagram showing schematic representations of several equilibrium fluid structures	16
2.2	Pseudoternary phase diagram of water/1-butanol/CTAB/octane system	18
2.3	Pseudoternary phase diagram of aqueous phase/1-butanol/CTAB/octane system	19
2.4	Variation of ΔG_M with radius of the droplet	24
2.5	Schematic representation of interdroplet exchange in water-in-oil microemulsions	27
2.6	Techniques for the synthesis of nanoparticles using microemulsions	30
3.1	Effect of components of microemulsion on radius of spontaneous curvature in water-in-oil microemulsions	38
3.1	Effect of components of microemulsion on critical radius due to interdroplet interaction in water-in-oil microemulsions	39
3.3	Effect of straight-chain alcohol cosurfactants on the solubilization of 0.05 M ferric nitrate solutions in microemulsions	44
3.4	Effect of branched-chain alcohol cosurfactants on the solubilization of 0.05 M ferric nitrate solutions in microemulsions	45
3.5	Maximum solubilization capacity of 0.05 M ferric nitrate solutions in microemulsions as a function of alcohol chain length	45

3.6 Effect of oil chain length on the solubilization of 0.05 M ferric nitrate solutions in microemulsions 46

3.7 Effect of surfactant chain length on the solubilization of 0.05 M ferric nitrate solutions in microemulsions 47

3.8 Effect of CTAB concentration on the solubilization of 0.05 M ferric nitrate solutions in microemulsions 48

4.1 Schematic representation of synthesis of ferric hydroxide in microemulsions 55

4.2 Differential thermal analysis of ferric hydroxide particles 57

4.3 Transmission electron micrograph of precursor iron hydroxide particles 58

4.4 Transmission electron micrograph of γ-Fe_2O_3 particles 59

4.5 X-ray diffractogram of iron oxide particles 60

4.6 X-ray diffractogram of cobalt ferrite particles 65

4.7 Transmission electron micrograph of cobalt ferrite particles 65

4.8 Magnetization loop for cobalt ferrite particles 66

5.1 Schematic representation of synthesis of barium-iron carbonate precursors in microemulsions 73

5.2 Transmission electron micrograph of barium-iron carbonate particles ... 76

5.3 Transmission electron micrograph of barium ferrite particles 77

5.4 Thermogravimetric analysis of precursor particles 78

5.5 Differential thermal analysis of precursor particles 79

5.6 X-ray diffractogram for barium ferrite particles 80

5.7 Magnetization loop for barium ferrite particles 81

5.8 Effect of Sn and Co doping on coercivity and saturation magnetization of barium ferrite particles 83

5.9 Transmission electron micrograph of $BaFe_{10.4}Co_{0.8}Sn_{0.8}O_{19}$ 84

6.1 UV-Vis absorbance for reactant and product microemulsions 92

6.2 Raw data for stopped-flow photometry of reactions in microemulsions . 93

6.3 Reproducibility of data obtained for stopped-flow photometry of reactions in microemulsions 94

6.4 Effect of droplet size of microemulsion on reaction rate for aqueous phase concentrations of (a) 0.5 mM, (b) 0.25 mM, and (c) 0.1 mM 98

6.5 Effect of aqueous phase concentration on reaction rate in microemulsions for (a) $\omega_o = 11.11$, and (b) $\omega_o = 4.44$ 99

6.6 Effect of straight chain alcohols on rate of reaction in microemulsions 101

6.7 Effect of branched chain alcohols on rate of reaction in microemulsions 102

6.8 Effect of oil chain length on rate of reaction in microemulsions 103

7.1 Recycling and re-use of organics for reaction in microemulsions 109

Abstract of Dissertation Presented to the Graduate School
of the University of Florida in Partial Fulfillment of the
Requirements for the Degree of Doctor of Philosophy

SYNTHESIS OF MAGNETIC OXIDE NANOPARTICLES USING MICROEMULSIONS

By

Vinod Kumar Pillai

August 1995

Chairperson: Dinesh O. Shah
Major Department: Chemical Engineering

There has been increasing scientific and technological interest in particles with nanometer size due to their unique properties and applications. Magnetic nanoparticles are of special interest due to their applications in magnetic recording media and magnetic fluids. Several techniques have been used to synthesize a variety of magnetic particles for these applications, with efforts to control their size, shape and size distribution. In this dissertation, nanoparticles of magnetic oxides such as γ-Fe_2O_3, cobalt ferrite, barium ferrite and doped barium ferrite have been synthesized using water-in-oil microemulsions. The nanosize droplets of water-in-oil microemulsions have been used as constrained reactors for the synthesis of hydroxide or carbonate precursors of these particles. These precursors have then been heat treated to produce the oxides. These oxide nanoparticles have been characterized by x-ray diffraction,

transmission electron microscopy and magnetic property measurements. Cobalt ferrite and barium ferrite nanoparticles thus synthesized were found to be essentially single domain, with high coercivity and saturation magnetization. Barium ferrite particles were also doped with tin and cobalt to reduce the coercivity. It is thus possible to obtain barium ferrite particles of any required coercivity, with little loss in magnetization by varying the composition of the dopants. The microemulsion systems used for synthesis reactions were characterized using solubilization experiments to select a suitable microemulsion for nanoparticle synthesis. A system with cetyl trimethyl ammonium bromide as surfactant, 1-butanol as cosurfactant and octane as the oil phase was found to have the maximum solubilization capacity. Reaction kinetics studies of these microemulsion systems revealed that chain length compatibility between cosurfactant, oil and surfactant is a significant factor in controlling the rate of the reaction. Chain length compatibility leads to a rigid interface which slows down the reaction rate considerably. The other important factor was the droplet size and aqueous phase concentration in microemulsion droplets. For high aqueous concentrations, reaction rate increased with decrease in droplet size of the microemulsion.

CHAPTER 1
INTRODUCTION

1.1 Importance of Nanoparticles

Particles with nanometer size in at least one dimension are of increasing scientific and technological interest [1]. There is clear evidence that small atomic clusters (10-1000 atoms) exhibit novel and hybrid properties between the molecular and bulk solid-state limits. These atomic clusters, or "nanoparticles," as they are sometimes called, have unique properties due to their strong chemical bonding and electron delocalization. The large fraction of atoms residing at the surfaces and grain boundaries of these materials also leads to materials with novel properties. Because of their ultrafine sizes, and surface cleanliness, these particles can easily overcome conventional restrictions of phase equilibria and kinetics, leading to lowering of sintering and solid-state reaction temperatures, and increase in sintering rate. Such nanoparticles are not only of basic physical interest, but have also resulted in important technological applications such as (a) catalysis, (b) high-performance ceramic materials, (c) micro-electronic devices, and (d) high density magnetic recording [1-3]. For example, the study of nanoparticles of transition metal atoms has helped researchers understand the origin of their unique chemical properties in correlation with their important catalytic applications [4]. Atomic clusters of semiconductor materials have hybrid molecular-

solid state properties as these particles are too small to have the bulk band structure [5]. This leads to unique electronic and optical properties.

Recently, the use of clusters in synthesizing consolidated materials is also being pursued actively [1]. This results in ultrafine-grained materials called "nanophase materials" [6-8] which may contain crystalline, quasicrystalline, or amorphous phases and can be metals, ceramics, or composites with rather unique and improved mechanical, electronic, magnetic and optical properties, than normal, coarse-grained polycrystalline materials. Also, new micro-homogeneous, multi-component composites with nanometer-sized microstructures can be synthesized by reacting, coating and mixing various types of nanophase materials [1].

1.2 Synthesis of Nanoparticles

In recent years, several techniques have been developed for the synthesis of various types of nanoparticles. A wide range of gas phase, vacuum methods, and liquid phase techniques have been used to synthesize metals, oxides, sulfides, carbides, nitrides, chlorides and other compounds [1-9].

Gas phase techniques involve volatilization of a monomer and then its condensation, in the presence of an inert gas or vapor, into nanoparticles. Uyeda [10] has extensively studied the direct evaporation of atomic clusters into a gas to produce an aerosol by using a heated crucible or oven. Mean particle diameters as small as 3-4 nm have been achieved with this technique and can be controlled by the length of the reactor and the flow of the inert gas. There are, however, some temperature limitations

on this process depending on the type of oven source used. Laser vaporization is another technique which has been used to volatilize monomers to produce nanoparticles of semiconductors [11], transition metals [12] and other metals [13]. In this method, oven temperatures up to 10000°C can be obtained on a very short time scale. Laser pyrolysis employs a CO_2 laser which is used to heat up a mixture of reactant gas and an inert carrier gas to produce a saturated vapor of monomers. These monomers nucleate and condense to form nanoparticles. This technique has been used by Haggerty *et al.*[14] to synthesize nanoparticles of Si, Si_3N_4 and SiC, and by Rice *et al.*[15] for the production of ZrB_2 and TiO_2 and Si/N/C powder [16] of 100 nm.

Vacuum methods involve sputtering a target with high energy ions (e.g. Ar or Kr) to eject atoms and clusters from a solid surface, or using laser ablation to vaporize cluster ions from solid surfaces. This method has been used for the synthesis of C and Si nanoparticles among other types of particles by Woste *et al.*[17], Gruen *et al.*[18] and Lineberger *et al.*[19]. Although gas phase and vacuum methods have the advantages of producing very small particles (below 10 nm) of high purity, with a low degree of agglomeration, in most cases, it is difficult to control particle size distribution due to the fast reaction times. Also, due to the high temperatures involved in these techniques, a large amount of energy is required in the preparation of nanoparticles.

Liquid phase methods offer versatility in producing a wide range of materials, with a variety of shapes, and a much better control of size distribution can be obtained. Liquid phase techniques may be broadly categorized as homogeneous or heterogeneous. In the former, the system consists of one phase and precipitation of the final product

takes place out of this phase. In heterogeneous methods, the system is composed of one or more phases prior to the precipitation of the final product.

Using homogeneous systems, Zsigmondy [20] obtained monodispersed gold sols by reading chloroauric acid with formaldehyde. A similar method was used by Takiyama [21] and Turkevich *et al.*[22] to obtain spherical monodispersed selenium [23,24], nickel [25], silver bromide [26], cuprous oxide [27], sulfur [28] and ferrous hydroxide [29]. Other methods such as precipitation from homogeneous solutions, sol-gel processing, freeze drying [9,30-33] have also been widely used and studied.

Precipitation from poor solvents such as ethanol has been used to synthesize sulfur [34], monodispersed AgCl [35], lead iodate [36], lanthanum iodate [37]. Matijevic *et al.*[38] have used decomposition with acids to synthesize cadmium sulfide [38], zinc sulfide [39], and lead sulfide [40]. Hydrolysis reactions have been used to synthesize $Al(OH)_3$ [41], α-Fe_2O_3 [42] and TiO_2 [43]. Berry *et al.*[44-46] have obtained monodispersed silver halides by introducing silver nitrates into gelatin solutions.

Although these liquid phase methods provide good control of size distribution, problems such as contamination, poor crystallinity and particle agglomeration still exist. Precipitation reactions in microemulsions offers a novel and versatile technique for the synthesis of a wide variety of nanoparticles with the ability to precisely control the size and shape of the particles formed [47-49]. The cage-like effect in microemulsions, where the droplets act as constrained nanosize reactors, limits particle nucleation, growth and agglomeration. This dissertation focusses on using water-in-oil

microemulsions to synthesize a variety of magnetic oxide nanoparticles which may have applications in high density particulate magnetic recording.

1.3 Nanoparticles for Magnetic Recording

Recording is the process of storing information in a suitable media so that it can be used (read-back or overwritten) again when required [217]. In magnetic recording, the information to be recorded, whether sound, image, or numerical data, is first converted to a time varying electrical current signal. This current is passed through the recording head which consists of a small coil and a gapped magnet which intensifies and localizes the resulting field. This gap is in close proximity to the recording medium which moves relative to the head. The recording medium consists of a magnetic material coated or deposited on the surface of a tape or a disk. The signal current creates a magnetic field in the head which magnetizes the coating such that the time varying input current signal is converted into a spatially varying magnetic pattern along the surface of the magnetic medium. This is the writing process. In the read-back process, the surface is again moved past the head, or past a different but similar head. Now, the field arising from the remanent magnetization of the surface magnetizes the gapped magnet, creating a magnetic flux through the coil around the head. The relative motion between the head and the medium gives rise to a time varying induced voltage which is changing with the spatially changing magnetization of the surface. This time varying voltage is the output signal. There are two distinct types of magnetic recording, longitudinal and perpendicular. In the former, the preferred axis of

magnetization of the magnetic media is parallel to the surface, while in the latter, it is perpendicular to the surface [217].

Ever since magnetic recording media were first prepared, extensive efforts have been made to produce improved magnetic dispersions [50-52]. The particles used for magnetic recording should have high saturation magnetization, an adequate coercivity, be single domain with a domain size small enough to record with satisfactory resolution and signal-to-noise ratio, but large enough to be thermally stable [53,54]. Development of small particles is important, since a higher number of particles per unit volume is needed for better signal-to-noise ratios [55]. In many of these applications it is desirable, or even essential, to employ particles uniform in size and shape. The magnetic oxides used extensively for particulate magnetic recording are γ-Fe_2O_3, Fe_3O_4, Co-doped γ-Fe_2O_3 and CrO_2 for longitudinal recording, and hexagonal ferrites like $BaFe_{12}O_{19}$ for high density perpendicular recording.

1.3.1 Requirements of Particulate Recording Media

Magnetic properties of a medium have a prime influence on its performance. This places some primary requirements on the magnetic materials to be used in recording media. Some of these requirements are discussed below.

1.3.1.1 Retentivity

The retained magnetization intensity, or retentivity (M_r) of the coated tape or disk should be sufficiently high, since it determines the strength of the field sensed by the read-back head and the amount of information that can be stored per unit volume.

The retentivity should not be too high or else the field would demagnetize adjoining tracks on the medium. The retained magnetization depends on the intrinsic magnetization of the magnetic material on the tape, and also on the preferred directions of magnetization of this material.

1.3.1.2 Coercivity

The field strength required to cause magnetic reversal in a magnetic material is called its coercivity, H_c. The coercivity of a recording media should be large enough to prevent unwanted changes, degradation or erasure of the signal during storage by small magnetic fields in the vicinity. On the other hand, coercivity should not be so large as to prevent successful writing, or erasure by available heads.

1.3.1.3 Switching field distribution

The coercivity of a magnetic material does not completely characterize its properties for recording properties. The breadth of the distribution of fields, centered on the coercivity, is also crucial. This can be expressed in a number of ways, one common way is to denote it as the switching field distribution (SFD). This is defined as the ratio of ΔH to H_c, where ΔH is the full width at half maximum of the dM/dH curve at H_c (see figure 1.1). A narrow SFD facilitates the writing of sharp, well-defined magnetic transitions, and therefore contributes to the ability to record information at high densities. A broad SFD not only diffuses the transitions, but it also can lead to easy erasure. Another parameter of importance is the squareness ratio (M_r/M_s), which should be close to one for higher retentivity.

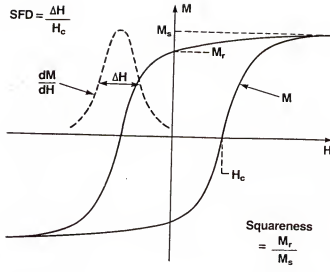

Figure 1.1 Hysteresis loop (plot of magnetization versus applied field) for a typical recording medium [217]

1.3.1.4 Anisotropy

In single domains, the uniform crystal lattice favors electron spin alignment and therefore magnetization in certain directions, while it discourages magnetization in other directions. The most favored magnetic direction is called the easy axis, whereas the least favored is called the hard axis. This phenomena is called magnetic anisotropy. When a domain is forced to reverse its direction of magnetization under the influence of a sufficiently strong external field, its magnetization has to pass through a hard axis. The greater the anisotropy, the more difficult the transition and higher the coercivity. The types of anisotropy affecting magnetic particles in recording media the most are

shape anisotropy and crystal anisotropy. Shape anisotropy is most important for magnetic tapes where acicular (needle shaped) particles of gamma ferric oxide, or chromium dioxide are used for magnetic tapes. These particles can be oriented in a preferred direction to increase the retentivity, the squareness ratio, and the SFD. Crystal anisotropy can be increased by doping materials. An example is the doping of gamma ferric oxide by cobalt which increases the crystal anisotropy and the coercivity of the material.

1.3.1.5 Particle Size

The magnetic characteristics of particles used for recording media depend crucially on their size and shape. These magnetic particles should be essentially single domain, i.e. all magnetic moments in the particle should magnetize in one direction. For any magnetic material there exists a critical size, d_{SD}, below which it remains single domain. There also exists a characteristic size of the particle, d_{SP}, below which the material becomes super-paramagnetic at the temperature of operation. Therefore, the size range over which a magnetic particle is useful in a storage medium is $d_{SP} < d < d_{SD}$. It is evident that narrower the particle size distribution, more particles would fall into the above size range and better the quality of the medium [56]. Therefore, the material used for a high quality recording medium should be ultrafine, chemically homogeneous, stable, with narrow particle size distribution and have a predetermined shape. These requirements demand a reliable and reproducible technique for their synthesis.

The difficulty of obtaining uniform-sized nanoparticles of magnetic oxides stems from the fact that their preparations are mostly done in bulk aqueous media in which it is difficult to control nucleation and grain growth. Conventional techniques for the preparation of fine particles include bulk precipitation, sol-gel processing, spray-drying, freeze-drying, hot-spraying, evaporation-condensation, matrix-isolation, laser induced vapor phase reactions and aerosols [31-33,57-59]. Generally, in most types of fine particles prepared by these methods, there is a polydispersity in the particle size distribution. In addition it is usually not possible to precisely control the size.

In order to try and overcome these difficulties, in the present work, constrained nanosize reactors such as the aqueous cores of water-in-oil microemulsions have been used for the formation of uniform sized, microhomogeneous nanoparticles of magnetic oxides.

1.4 Thesis Organization

This thesis has been organized into seven chapters. The present chapter gives an introduction to the importance of nanoparticles, their applications and a brief description of various synthesis routes. Chapter 2 presents an overview of microemulsions and a literature review on the synthesis of nanoparticles using microemulsions. Solubilization experiments for the characterization of microemulsion systems used for nanoparticle synthesis is described in Chapter 3. Chapter 4, describes the synthesis of γ-Fe_2O_3 and cobalt doped iron oxide using water-in-oil microemulsions and discusses the characterization and magnetic properties of these nanoparticles.

Chapter 5, describes the synthesis of barium ferrite and tin and cobalt doped barium ferrite using water-in-oil microemulsions and discusses the characterization and magnetic properties of these nanoparticles. Chapter 6 describes stopped-flow experiments used to measure reaction kinetics in microemulsion systems used for nanoparticle synthesis. Chapter 7 contains the conclusions of this dissertation along with some recommendations for future work which include ideas about scale-up of this process using recycle and re-use of the organics.

CHAPTER 2
MICROEMULSIONS AND SYNTHESIS OF NANOPARTICLES

2.1 Introduction

A microemulsion is generally defined as a thermodynamically stable, isotropic dispersion of two relatively immiscible liquids, consisting of microdomains of one or both liquids stabilized by an interfacial film of surface active molecules [60]. Microemulsions may be classified as water-in-oil (w/o) or oil-in-water (o/w) depending on the dispersed and continuous phases. In both cases, the dispersed phase consists of monodispersed droplets in the size range of 10 - 100 nm [61].

Microemulsions were first introduced by Schulman and his co-workers in 1943 [62]. They attributed the spontaneous formation of microemulsions with the uptake of water or oil due to the negative transient interfacial tension which allows the free energy to decrease as the total oil-water interfacial area increases [62,63]. They explained that if the surface tensions were positive, the ultimate equilibrium condition for these systems would be to separate out into two phases. This is the usual case with macroemulsions. However, if the interfacial tension becomes negative due to the surface pressure of the interfacial film being greater than the interfacial tension between the water and oil phases, then the equilibrium is reverse and the interfacial area tends towards its greatest value. This will necessitate one phase to break up into the greatest

dispersion of droplets according to the maximum interfacial area which can be produced by the available interphase molecules. The negative interfacial tension produced by the mixing of the components becomes zero or a very small positive number of the order of 10^{-2}-10^{-3} mN/m, and the dispersion does not separate at equilibrium.

During the past fifteen years, studies on both theoretical and experimental aspects of microemulsions have provided a better understanding of the formation, properties, and phase behavior of microemulsions [64-70]. Due to their importance in various technological applications such as enhanced oil recovery, pharmaceutics, and cosmetics, the structure and structural transitions of microemulsions have been extensively studied using x-ray and light scattering, ultracentrifugation, spin label probes, dielectric relaxation, fluorescence probes, and neutron scattering [71-83]. Hou *et al.* [84] and Leung *et al.* [85] have studied the solubilization capacity and phase equilibria of water-in-oil microemulsions. They have considered two phenomenological parameters, namely the radius of spontaneous curvature of the interface and elasticity of interfaces to formulate the theory and interpret the experimental results. They showed that solubilization and phase equilibria were affected by the molecular structure of the interface which in turn depends on the structure of the oil, alcohol (co-surfactant), surfactant, and salinity of the aqueous phase.

As many applications depend on the dynamics of microemulsions, the characterization of the size and shape of microemulsion droplets and their inter-droplet interaction has been vigorously pursued recently. Many techniques such as light

scattering, small angle neutron scattering, fluorescence quenching, stopped-flow, and electrical conductivity have been used to study the dynamics of microemulsions [86-92].

Microemulsions are industrially relevant due to their applications in a number of areas [47]. The interfacial and rheological properties of microemulsions are important to exploit surfactant-enhanced tertiary oil recovery methods. There are also obvious applications in the food and cosmetics industries, particularly using phospholipid surfactants. The ability to precisely control the size and stability of the microstructure domains of microemulsions makes them useful for applications in liquid membrane technology [47,93]. Microemulsions also provide compartmentalized liquid structures having high surface area and can therefore be used as novel and versatile media for chemical synthesis. This is significant for potential applications in enzymic reactions in microemulsions [93]. Not only do enzymes retain their activity in microemulsions, but in water-in-oil microemulsions, the thermodynamic equilibrium of reactions is shifted so as to favor reactions in the reverse direction as compared to aqueous solution. Another potential use of the fluid but structured microdomains of microemulsions is in the preparation of sub-micron or nano-particles of a desired size or shape, reflecting the structure and environment of the aqueous droplets.

2.2 Microstructure of Microemulsions

The microstructure of microemulsions has been studied by a variety of techniques such as x-ray diffraction [71], dielectric relaxation, ultracentrifugation [75], fluorescence probes [77], neutron scattering [82,83], electron microscopy [94], and

recently by cryo-transmission electron microscopy [95]. Microemulsions have generally been described as spherical droplets with diameters ranging from 10 to 100 nm, with droplets of oil dispersed in water (o/w microemulsion) or droplets of water dispersed in oil (w/o microemulsion). It has now been shown that when microemulsions contain comparable amounts of oil and water, some of these systems may show a bicontinuous structure [96,97]. Some microemulsions have also been known to show a cubic structure [98].

Polydispersity effects have been noted qualitatively in several studies on water-in-oil microemulsions [99]. It was noted that if the interfacial film of the microemulsion is flexible, the radius of the droplets is not strictly fixed but is distributed around an average value (polydispersity) and that the shape of the droplets fluctuates. The droplets of a microemulsion can also be deformed by external perturbations. These deformations may result from thermal fluctuations or due to fluctuations in magnetic field in the case of diamagnetic surfactants [99].

Figure 2.1 shows an idealized ternary phase diagram of an oil-water-surfactant system where several equilibrium fluid structures have been illustrated. As one moves along the water-surfactant or oil-surfactant sides of the triangle, the surfactants can spontaneously self-organize to form micelles or reverse micelles at low surfactant concentrations. As the surfactant concentration is increased, a variety of liquid crystalline structures are formed. These micelles and reverse micelles also swell to form o/w and w/o microemulsions respectively as the concentration of oil and water is increased. The phase inversions from o/w to w/o microemulsions involves, in some

systems, transitions from an isotropically clear phase to a turbid (two phase) region, back to a clear phase. However, in other cases, the phase inversion may be continuous and clear as the system goes through a transition to a bicontinuous or cubic phase microemulsion. This was first imagined by Scriven [97] who suggested that in these cases oil and water form two intertwined networks separated by an interfacial film of surfactants. Hence, in this situation, droplets, globules or aggregates can no longer be defined.

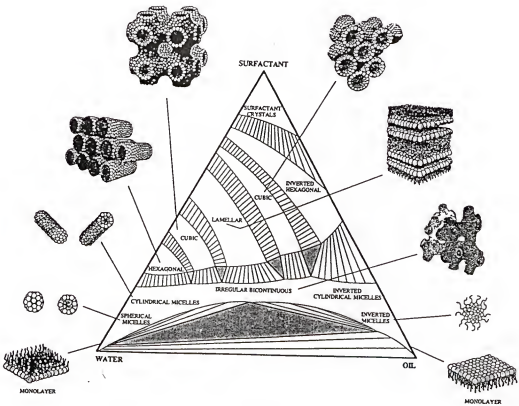

Figure 2.1 Idealized ternary phase diagram showing schematic representations of several equilibrium fluid structures [95]

2.3 Phase Behavior and Solubilization in Microemulsions

The phase behavior and solubilization capacity of microemulsions depend upon many factors such as salinity [84], temperature [100-102], composition [84,100-102], structure of oil phase [84,100-102,104,105], type of surfactant [84,102] and cosurfactant [84,101,105-107]. The solubilization capacity of microemulsions is primarily related to the size of the droplets at the limit of solubilization where phase separation is first observed. Thermodynamically, the equilibrium radius at this point is related to their free energy. Therefore, several researchers have used a thermodynamic approach to study solubilization in microemulsions. Ruckenstein *et al.*[107] used this approach to analyze solubilization in both w/o and o/w microemulsions by considering the balance between dispersion entropy and interfacial tension. Their predictions were in qualitative agreement with experimental results. Another approach used was to consider the equilibrium of microemulsions that coexist with excess fluid by stressing the importance of the curvature of the interface [108-110]. The results of all the above studies showed correlations between the chemical structure of the components of the microemulsion to its solubilization capacity. They predicted that solubilization capacity increased in o/w microemulsions and decreased in w/o microemulsions as salinity was increased, or the area of polar head group decreased, or oil chain length decreased, or surfactant/ cosurfactant ratio increased. These predictions are in good agreement with most experimental results where phase equilibrium is dominated by the curvature of the interface. In other systems, phase equilibrium and solubilization is influenced by entropic contributions [111] and attractive interdroplet interactions [112-116].

Figure 2.2 depicts a pseudo ternary phase diagram for a water/cetyl trimethyl ammonium bromide (CTAB)/1-butanol/n-octane system showing the water-in-oil (L_2) and oil-in-water (L_1) microemulsion regions. When a salt is dissolved in the water phase of this system, the water-in-oil microemulsion region (L_2) becomes much larger as seen in figure 2.3 [117]. In this system, the interdroplet interactions, rather than the curvature of the interface seem to influence the solubilization capacity. This system is similar to the ones used for nanoparticle synthesis in this thesis. A detailed discussion of these systems is given in Chapters 3 and 6.

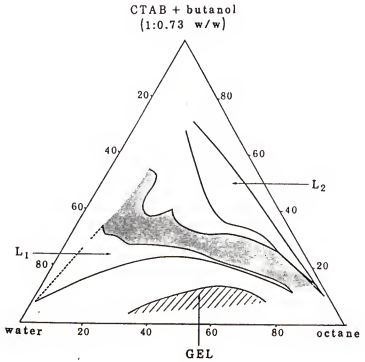

Figure 2.2 Pseudoternary phase diagram of water/1-butanol/CTAB/octane system [117]

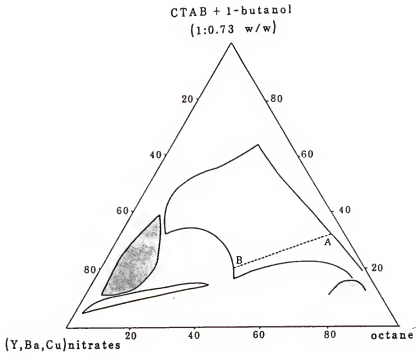

Figure 2.3 Pseudoternary phase diagram of aqueous phase/1-butanol/CTAB/octane system [117]

2.4 Thermodynamic Stability of Microemulsions

Microemulsions are formed spontaneously on mixing various components in the required ratio (obtained from phase diagrams) and remain as a stable single phase as long as there are no drastic changes in the temperature, pressure or composition. This is in contrast to emulsions (or macroemulsions) which require considerable energy input (shaking, stirring, sonicating) for their formation and will eventually phase separate even with no changes in temperature, pressure or composition. This is why microemulsions are termed to be thermodynamically stable.

The primary requirement for the formation of a microemulsion is the existence of ultralow interfacial tension at the oil-water interface. To achieve this, sometimes a cosurfactant has to be added. It has been suggested that the existence of a large amount of surfactant and cosurfactant at the interface may induce a very high spreading pressure large enough to produce negative interfacial tensions. This negative interfacial tension was used to explain the spontaneous formation of microemulsions [63,94,118-121]. However, as shown by Miller and Scriven [122], this explanation may be an oversimplification as it ignores other factors which could, in principle, contribute significantly to the energy change that accompanies a small deformation of the interface while the interfacial tension is still positive but small. One of these factors is the entropy effect caused by the diffuse electrical double layers near the interfaces. They explained that for a plane interface, the destabilizing effect of a diffuse layer is primarily that of a negative contribution to the interfacial tension. In such circumstances, total interfacial tension, including the contribution of the diffuse layer, is approximately zero at marginal stability. Their analysis showed that qualitatively similar results were obtained for spherical interfaces also. Thus, dispersion is initiated by fluctuations and instability caused by the interfacial configuration of these low tension systems.

Ruckenstein *et al.*[66] have explained the thermodynamic stability of microemulsions by calculating free energy changes due to interfacial tension, interaction among droplets and entropy of dispersion. Thus the free energy change due to dispersion (assuming negligible volume change on mixing) can be expressed as

$$\Delta G_M = \Delta U_M - T\Delta S_M \qquad [2-1]$$

The free energy change, ΔG_M, consists of changes in the interfacial free energy, ΔG_1, the interaction energy among the droplets, ΔG_2, and the effect caused by the entropy of dispersion, ΔG_3. The interaction forces considered here are the van der Waals attraction forces and the electrical double layer repulsive forces. The competition among the various terms contributing to the free energy change determines whether or not microemulsions can form.

If the droplets are assumed to be spherical, the increase in the free energy caused by the creation of interfacial area is given by

$$\Delta G_1 = 4\pi R^2 m (f_s + f_d) \qquad [2-2]$$

where R is the radius of the droplet, f_s the specific surface free energy of the uncharged surface, f_d the specific free energy for the formation of the double layers and m is the total number of droplets related to the volume of the dispersed phase, ϕ_2, by the relation

$$m = \frac{\phi_2}{v} \qquad [2-3]$$

The value of f_d can be found using the Debye-Huckel approximation, while, f_s is equal to the surface tension for a single component system.

The free energy change due to interaction among droplets depends on the interaction potential, U, and can be given by

$$\Delta G_2 = \frac{m}{2} U \qquad [2-4]$$

The interaction potential of a particular droplet with all other droplets can be given by

$$U = \frac{m}{V_c} \int_{2R'}^{\infty} u(r)\, g(r)\, 4\pi r^2 dr \qquad [2-5]$$

where g(r) is the radial distribution function, u(r) is the pair potential, V_c is the volume of the mixture and 2R' is the average distance between the centers of two nearest droplets. The pair potential, u(r), is composed of two parts, the van der Waals attraction potential, and the electrical double layer repulsive potential.

The increase in disorder, leading to an increase in entropy of the system upon dispersion can be obtained by the entropy of mixing given by

$$\Delta S_M = k \ln \Omega \qquad [2-6]$$

where Ω represents the number of configurations of a liquid mixture formed from N_1 molecules of the continuous phase and N_2 molecules of the dispersed phase, the latter being in the form of *m* equal sized droplets. Lattice models have been used to evaluate Ω and determine the upper and lower bounds for ΔS_M.

The variation of ΔG_M with the radius of the droplet, R, has thus been determined at constant values of ϕ_2 using

$$\Delta G_M(R) = \Delta G_1 + \Delta G_2 - T\Delta S_M \qquad [2-7]$$

When the free energy, ΔG_M, is negative, spontaneous formation of microemulsions occurs. When ΔG_M is positive, emulsions can be produced, which although thermodynamically unstable, may be kinetically stable. The value of R which yields the minimum of ΔG_M, denoted by R^*, is the most stable droplet size for a given volume fraction of the dispersed phase and may be obtained from

$$\frac{d\Delta G_M}{dR} = 0 \qquad [2-8]$$

if the following condition is satisfied at $R=R^*$.

$$\frac{d^2\Delta G_M}{dR^2} > 0 \qquad [2-9]$$

Using these equations, Ruckenstein *et al.*[66] obtained curves for free energy as a function of radius of droplets, R (see figure 2.4). For cases C and D, the free energy is always positive and therefore, thermodynamically unstable emulsion are formed. For cases A and B, the free energy change is negative within a certain range of R, and therefore any dispersion of droplets having a radius within this size range forms thermodynamically stable microemulsions.

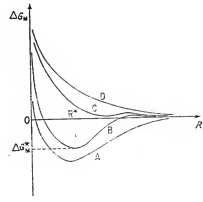

Figure 2.4 Variation of ΔG_M with radius of the droplet [66]

Several other studies have also been directed towards constructing thermodynamic models for microemulsions. These can be divided into two main groups. The first one is a phenomenological approach, initiated by Talmon *et al.*[123] and further developed by De Gennes *et al.*[68,111] and Widom [124]. This approach considers the oil and water phases as continuum liquids, and the interface as a flexible sheet similar to insoluble Langmuir monolayers [125]. The presence of salt and alcohol are not treated directly, but through energy parameters affecting the interface. In these models, the free energy is calculated as a function of composition for a hypothetical homogeneous phase. This can then be used to generate phase diagrams. Recently, Andelman *et al.*[126] have improved on these models by considering the interface to

be an incompressible two-dimensional fluid and improving the treatment of the bending energy of the interface.

The second approach is based on the construction of microscopic lattice models in which a cell of the lattice contains only a small number of molecules. This approach was initiated by Wheeler *et al.*[127] and was later extended by Widom [128], Schick *et al.*[129] and Chen *et al.*[130].

2.5 Dynamic Structure and Reactions in Microemulsions

Microemulsions have been shown to have a dynamic structure wherein the droplets of the dispersed phase are diffusing through the continuous phase and colliding with each other. These collisions are inelastic and have been termed "sticky collisions" as the droplets coalesce and temporarily merge with each other but subsequently break to form separate droplets [88-90,131-138]. The average size and number of droplets remains the same as a function of time. Like all colloidal suspensions, the droplets in microemulsions are strongly influenced by inter-droplet forces arising due to London-Van der Waals forces and electrostatic forces. In o/w microemulsions, the latter is the dominant force as the polar head groups face the exterior of the droplets [139-141]. In w/o microemulsions, as the continuous phase is hydrophobic, electrostatic forces are expected to be negligible. However, the strengths of these attractive forces have been found to be two to three orders of magnitudes higher than that obtained from theoretical calculations of Van der Waals forces of attraction [142-144].

Two mechanisms have been suggested to explain the origin of attractive interactions. Lemaire *et al.*[52mm] argued that for water-in-oil microemulsions, the tails of the surfactant molecules residing on two different droplets prefer to interpenetrate each other rather than to be in contact with the oil. The penetration depth depends on the length of the cosurfactant. The overlapping of the surfactant films and the increased proximity of the water cores result in an increase of the van der Waals attraction. This mechanism assumes that the droplets remain undeformed.

Safran [17mm] observed that a spherical droplet is unstable with respect to shape fluctuations which lower the bending energy when the spontaneous curvature of the film is much less than the actual curvature of the film. Under such conditions, the fusion of two droplets into a dimer at constant surface area and volume lowers the curvature energy. This mechanism is applicable to both water-in-oil and oil-in-water microemulsions, however, it does not explain attractions observed in microemulsions made with lipophilic surfactants. Thus each mechanism alone cannot explain attractive interactions between droplets in microemulsions, but both mechanisms together may explain most of the experimental observations.

In water-in-oil microemulsions, the continuous collisions of the aqueous droplets leads to coalescence and breaking apart of droplets resulting in a continuous exchange of solute content [90,132]. A schematic representation of this process is shown in figure 2.5.

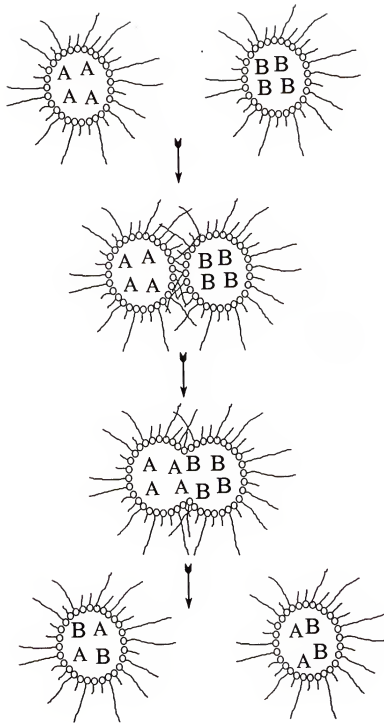

Figure 2.5 Schematic representation of interdroplet exchange in water-in-oil microemulsions

The frequency of collisions depends upon the diffusion of the aqueous droplets in the continuous media, i.e. oil, while the exchange process depends on the attractive interactions between the surfactant tails and the rigidity of the interface, as the aqueous droplets collide with each other [90]. It is important to recognize that every collision between two droplets may not result in coalescence of two droplets. The fraction of collisions resulting in successful coalescence depends on the surface rigidity or surface elasticity. Thus, depending on the components of the system, we can have conditions ranging from perfectly elastic collisions (i.e. no coalescence) to perfectly inelastic collisions (all collisions result in coalescence).

For reactions in water-in-oil microemulsions involving reactant species totally confined within the dispersed water droplets, a necessary step prior to their chemical reaction is the exchange of reactants by the coalescence of two droplets. When chemical reaction is fast, the overall reaction rate is likely to be controlled by the rate of coalescence of droplets [90]. Therefore, properties of the interface such as interfacial rigidity are of major importance. A relatively rigid interface decreases the rate of coalescence, and hence leads to a low reaction rate. On the other hand, a substantially fluid interface in the microemulsion enhances the rate of reaction. Thus, by controlling the structure of the interface, one can change the reaction kinetics in microemulsions by an order of magnitude [145]. It has been further shown that the structure of oil, alcohol and ionic strength of the aqueous phase can significantly influence the rigidity of the interface and the reaction kinetics [86,145].

Conceptually, if one takes two identical water-in-oil microemulsions and dissolves reactants A and B, respectively, in the aqueous phases of these two microemulsions, upon mixing, due to collision and coalescence of the droplets, the reactants A and B come in contact with each other and form AB precipitate. This precipitate is confined to the interior of the microemulsion droplets and the size and shape of the particle formed reflects the interior of the droplet. This is one of the principles utilized in producing nanoparticles using microemulsions (see figure 2.6a). However, nanoparticles can also be produced in microemulsions by the adding a reducing or precipitating agent, in the form of a liquid or a gas, to a microemulsion containing the primary reactant dissolved in its aqueous core. Figure 2.6b shows the formation of metallic nanoparticles by adding reducing agents such as hydrazine or hydrogen gas in the microemulsion containing the metal salt. Figure 2.6c shows the formation of oxide, hydroxide or carbonate precipitates by bubbling gases like O_2, NH_3, or CO_2 through a microemulsion containing soluble salts of the cations. In the past decade or so, several researchers have used these techniques to synthesize nanoparticles in microemulsions. These articles are briefly described in the next section.

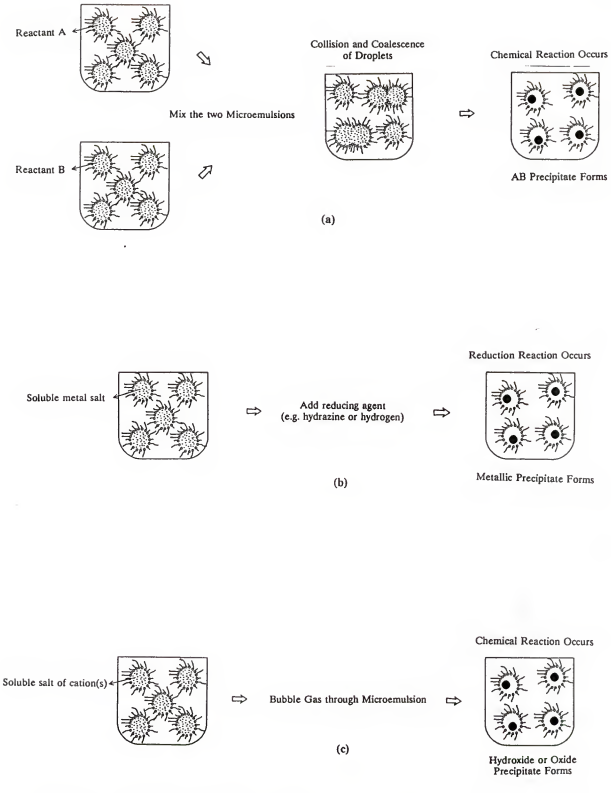

Figure 2.6 Techniques for the synthesis of nanoparticles using microemulsions

2.6 Particle Synthesis in Microemulsions

Synthesis of ultrafine particles using reactions in microemulsions was first reported by Boutonnet *et al.*[48] when they obtained monodispersed metal particles (in the size range 3-5 nm) of Pt, Pd, Rh and Ir by reducing corresponding salts in water pools of water-in-oil microemulsions with hydrazine or hydrogen gas (see also reference 108). Since then, there have been several reports in literature where microemulsions have been used for the synthesis of a variety of nanoparticles.

Metallic nanoparticles and metal clusters have a wide range of applications, including their use in catalysis, as biological stains, and as ferro-fluids. Touroude *et al.*[147] synthesized bimetallic particles of platinum and palladium by reduction of H_2PtCl_6 and $PdCl_2$ with hydrazine in water/pentaethylene glycol dodecyl ether/hexadecane microemulsions. Similarly, platinum particles have also been synthesized in aerosol-OT (AOT) and cetyl trimethyl ammonium bromide (CTAB) based microemulsions for applications in catalysis [148,149]. Colloidal gold and silver particles have potential applications as condensers for electron storage in artificial photosynthesis. This has led to studies by Kurihara *et al.*[150] on laser and pulse radiolytically induced colloidal gold formation in w/o microemulsions. Wilcoxon *et al.*[151] have used laser photolysis for the synthesis of gold nanoparticles. Colloidal gold and silver particles have also been synthesized by reduction of corresponding metal salts in water-in-oil microemulsions using sodium borohydride [152,153]. Pileni *et al.*[154] have synthesized metallic copper nanoparticles using copper substituted AOT surfactant in water-in-oil microemulsions.

Colloidal semiconductor particles, especially cadmium sulfide, have invoked a lot of interest due to their unique photochemical and photophysical properties. These properties are drastically dependent on the size of the semiconductor nanoparticles. Several researchers have therefore used water-in-oil microemulsions for the synthesis of such nanoparticles. Meyer *et al.*[155] have generated platinized colloidal cadmium sulfide *in situ* in AOT based microemulsions. Several studies have recently been published on the synthesis, growth and characterization of cadmium sulfide [49,156-165] and cadmium selenide [166] particles in microemulsions.

Colloidal particles of calcium carbonate, stabilized by surfactants, constitutes an important class of additives for oils used in lubrication for internal combustion engines. Water-in-oil microemulsions thus provide an ideal media for the synthesis of such particles. This has been exploited for the synthesis of calcium carbonate [167-170], barium carbonate [171], and strontium carbonate [172] particles by carbonation of their respective salts or hydroxides in the aqueous cores of water-in-oil microemulsions.

Microemulsions have also been used for the synthesis of monodisperse particles of nickel, iron and cobalt boride particles, which have applications in heterogeneous catalysis, by the reduction of metal salts using sodium borohydride [173,174]. Other nanoparticles synthesized in water-in-oil microemulsions include monodisperse silica particles [175-180], ellipsoidal, monodispersed basic copper sulfate nanoparticles [181], ultrafine TiO_2 particles [182], $Al(OH)_3$ particles [183], nano-size molybdenum sulfide particles [184], and magnetic particles such as magnetite [185,186] and maghemite [187].

In recent years, Shah *et al.*[117,188-195] have been successful in synthesizing a variety of nanoparticles using different microemulsion systems. These include *in situ* synthesis of nanoparticles of AgCl [188] and AgBr [189]; and microemulsion mediated synthesis of highly dense and microhomogeneous Y-Ba-Cu-O (123) and B-Pb-Sr-Ca-Cu-O (2223) high temperature ceramic superconductors [117,190,191], high coercivity barium ferrite for high-density perpendicular recording [191,192], superparamagnetic γ-Fe_2O_3 nanoparticles [193], zinc oxide based varistors [194] and TiO_2 nanoparticles [195]. The synthesis and characterization of nanoparticles of γ-Fe_2O_3 and barium ferrite using microemulsions is described in Chapters 4 and 5.

CHAPTER 3
MICROEMULSION CHARACTERIZATION

3.1 Introduction

Microemulsions are isotropic mixtures of oil and water, stabilized by an interfacial layer of surfactant (and cosurfactant). They consist of droplets of one phase dispersed in the other. In water-in-oil microemulsions, water or aqueous droplets are dispersed in the continuous oil (hydrophobic) phase. In these systems, the solubilization of water or aqueous phase is known to be influenced by the chemical structure of the oil, surfactant and cosurfactant used [104,105]. It has been shown that there exists a preferred oil chain length which solubilizes more water for a specific surfactant/alcohol pair than others [104]. Johnson *et al.*[105] have shown that in microemulsions with AOT (anionic) as the surfactant and Span-20 (nonionic) as the cosurfactant, the solubilization of water reached a maximum at a certain value of the surfactant/cosurfactant ratio. Similar results were reported by Leong *et al.*[196] using acrylamide as cosurfactant.

3.2 Theoretical Aspects of Solubilization

From a theoretical consideration, the solubilization capacity of water is related to the radius of microemulsion droplets, which is then thermodynamically related to the

stability of microemulsions. For a microemulsion composed of *n* spherical droplets of identical radius, the following expression has been formulated [84];

$$n_s A = n 4\pi R^2 \qquad [3-1]$$

$$n_s v_s + n_w v_w = n (4\pi R^3)/3 \qquad [3-2]$$

where n_s and v_s are the number and individual volume of the surfactant molecule, n_w and v_w are the number and volume of a water molecule, R and A are the external radius and the external interfacial area occupied by each surfactant molecule. From the above equations, the ratio of number of water to surfactant molecules can be written as

$$n_w/n_s = AR/(3v_w) - v_s/v_w \qquad [3-3]$$

In general, A is a very weak function of the radius for reasonably large R and tends toward a well-defined limiting value on approaching saturation of solubilization [68,202,203]. Thus, n_w/n_s is proportional to the radius of microemulsion droplets, as has been experimentally observed [204,205]. Using values obtained at saturation, the solubilization capacity can be defined as

$$(n_w/n_s)_{sat} = A_{sat}R_{sat}/(3v_w) - v_s/v_w \qquad [3-4]$$

Therefore, the stability of a microemulsion against phase separation has to be examined in order to determine the value of R_{sat}. The basic thermodynamic treatment on the stability of microemulsions was initiated by Ruckenstein *et al.*[66,107,197]. In general, the free energy of a microemulsion is primarily decided by the entropic contribution of the dispersion of the droplets in the continuous phase, the interfacial curvature effect and the interaction between droplets [66,107,197-200]. Among the above considerations, the curvature of the interface and the interaction between droplets are strongly influenced by the molecular structures of the interfacial layer (surfactant and cosurfactant) and the continuous phase [50,68,201]. Based on this, two types of phase separations have been reported in literature [50,111-113,116,198,201, 206-209], the first one induced by curvature and the second induced by attractive interaction among microemulsion droplets.

3.2.1 Curvature Effect in Microemulsions

The importance of the curvature effect in the equilibrium between a water-in-oil microemulsion and excess water has been extensively studied [50,111,116,198,199,206]. This effect arises because adjacent polar heads interact differently from adjacent hydrocarbon chains leading to non-uniform interaction across the interfacial layer. This results in an interfacial bending stress which can cause a flat film to curve. At an equilibrium condition with negligible interfacial tension, an interface would assume an optimal curvature, $1/R_0$, known as spontaneous curvature [68,211]. The curvature effect thus reflects the tendency of the surfactant interface to bend towards oil or water

through the radius of spontaneous curvature [84]. For a single phase of identical spherical droplets, the interfacial free energy per unit volume f_i can be written as [68,116,210-212]

$$f_i = (3\phi/R)\,[\gamma + 2K(1/R - 1/R_o)^2] \qquad [3-5]$$

where R is the actual radius of the droplets, R_o the radius of spontaneous curvature of droplets, ϕ the volume fraction of droplets, and K is the rigidity constant of the interface [68,116,210].

Safran *et al.*[116] have shown that when curvature effect is dominant, phase separation occurs whenever R approaches R_o. The physical origin of this phase separation exists in the interfacial energy being minimized for $R \cong R_o$. For a small volume fraction of water, droplets with radius $R < R_o$ are formed. The radius of droplets grows as water is added. When R reaches R_o, the curvature energy can be minimized by expelling the excess water into a separate phase so that all droplets are constrained to an optimum size, R_o.

Mukherjee *et al.*[108] and Jeng *et al.*[109] have shown the influence of the chemical structure of the components on the spontaneous curvature of droplets. In water-in-oil microemulsions, it was found that the radius of spontaneous curvature decreases (and hence the solubilization capacity of water decreases), as the chain length of oil decreases, the chain length of cosurfactant increases, or the size of the polar head decreases. For systems where phase instability is induced by the curvature effect leading to the coexistence of microemulsion phase and excess water, the results can be summarized as shown in figure 3.1.

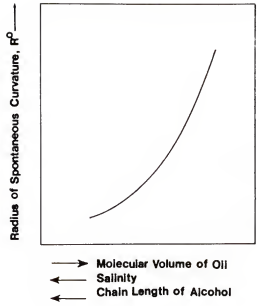

Figure 3.1 Effect of components of microemulsion on radius of spontaneous curvature in water-in-oil microemulsions [84]

3.2.2 Attractive Interaction between Microemulsion Droplets

Experimentally, phase separation has also been observed in microemulsions which leads to the coexistence of two microemulsion phases having the same continuous phase. These systems are characterized by a large interaction between the microemulsion droplets.

If the solubilization process is seen as a combination of the growth of microemulsion droplets and the mixing of these droplets with the continuous oil, then, in the initial stage of solubilization the droplets are small, and therefore stable for binary mixing. However, as the volume of water solubilized increases, the droplets will

grow as indicated in equation 3-1. At a certain point, the droplets will reach a critical value R_c fulfilling the condition for binary mixing. Beyond this critical point, the binary mixture of these droplets and continuous oil becomes unstable and separates into two phases of droplets with the same continuous phase. The critical droplet radius R_c increases as the penetrable length of the interfacial layer during collisions decreases, or with decrease in the molecular volume of the oil. It may also be affected by the chain length of the alcohol (cosurfactant) and salinity as shown in figure 3.2. The critical radius R_c increases with decrease in oil chain length, increase in alcohol chain length and increase in salinity.

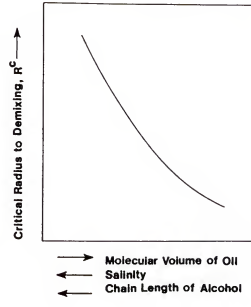

Figure 3.1 Effect of components of microemulsion on critical radius due to interdroplet interaction in water-in-oil microemulsions [84]

3.2.3 Solubilization Capacity in Microemulsions

For a system with a very rigid interface, the attractive interdroplet interaction is very small. Therefore, it may be neglected when compared to the curvature effect. Therefore, the radius of spontaneous curvature would be the limiting factor in this case. Solubilization can be improved in such systems by decreasing the spontaneous curvature of the interfacial film by making the interface more fluid (e.g. by using a cosurfactant with a shorter chain length, or by increasing the amount of cosurfactant, or replacing the continuous component with larger oil molecules). However, this will also increase the interdroplet attraction between droplets. So, this improvement will be limited as the increasing value of R_o meets the decreasing value of R_c. Hence, there would exist a maximum solubilization of water in a microemulsion to be determined by the various components of the microemulsion which in turn determine the radius of spontaneous curvature and the critical radius for interdroplet attraction. Thus, a systematic change in the amount and structure of the oil and cosurfactant can be used to determine the maximum solubilization for a microemulsion system. The experimental studies to measure the maximum solubilization described in the following sections are explained on the basis of the above discussions.

3.3 Experimental Procedure

For the synthesis of magnetic oxide nanoparticles, a suitable microemulsion system had to be selected, which would serve as a reaction medium for the precipitation

reactions. The main criteria for selection of a microemulsion system were that (a) the microemulsion should solubilize a large volume of aqueous phase so that the yield of the reaction is high, and (b) the components of the microemulsion (surfactant and oil) should not interact with the reactants and hinder the reaction. The presence of Fe^{3+} ions in all magnetic oxides led to the exclusion of commonly used anionic surfactants such as Aerosol OT as they are known to react with Fe^{3+} ions and precipitate. Also, water-in-oil microemulsions with nonionic surfactants are known to solubilize low volumes of aqueous phase. Therefore, a cationic surfactant was selected for the microemulsion system. Water-in-oil microemulsions with cetyl trimethyl ammonium bromide (CTAB) as surfactant and a short chain alcohol as co-surfactant are known to solubilize large volumes of aqueous phase [213]. This system was the basis for all experimental studies described in this chapter.

3.3.1 Materials

Ferric nitrate, cetyl trimethyl ammonium bromide (CTAB), tetradecyl trimethyl ammonium bromide (C_{14}TAB), dodecyl trimethyl ammonium bromide (C_{12}TAB), 1-propanol, 1-butanol, 1-pentanol, 1-hexanol, iso-butanol, iso-pentanol, tert-pentanol, n-heptane, n-octane, n-decane, n-dodecane, n-hexadecane (all technical grade) were purchased from Fisher Scientific. All reagents were used without further purification. Water was deionized and distilled before use. All experiments were carried out at room temperature.

3.3.2 Methods

Solubilization studies were conducted on various microemulsion systems to determine the optimum composition for maximum solubilization of ferric nitrate salt solutions in microemulsions. The solubilization capacity of ferric nitrate solutions was determined by gradually adding it to a mixture of surfactant, alcohol and oil under constant stirring. The solubilization capacity was taken as that point where the first visual evidence of phase separation occurred. (The microemulsion becomes turbid and separates into two phases after some time). The solubilization capacity "ω_o" has been defined as

$$\omega_o = \frac{moles\ of\ ferric\ nitrate + moles\ of\ water}{moles\ of\ surfactant} \qquad [3-6]$$

$$z = \frac{moles\ of\ cosurfactant}{moles\ of\ surfactant} \qquad [3-7]$$

3.4 Results and Discussion

Initial studies were made on the ferric nitrate (0.05 M)/CTAB/1-butanol/octane microemulsion system. The quantity "z" was varied (while keeping the concentration of CTAB in oil constant at 0.5 M) and the solubilization capacity of 0.05 M ferric nitrate solution was measured at various ratios (see figure 3.3 for the result). The solubilization capacity increased up to z=5 and then decreased. This indicates that there are two mechanisms controlling the solubility in this system, one for $z \leq 5$ and the other

for $z \geq 5$. When $z \leq 5$, as more cosurfactant (1-butanol) is added to the system, it resides at the oil-water interface until saturation is reached at z=5. This increases the interfacial area, thus decreasing the curvature of the interface, and increasing the radius of the droplets and facilitating the solubilization of more ferric nitrate solution. The curvature effect is dominant up to this point. There is a critical droplet radius for each value of z beyond which the aqueous phase is expelled out causing phase separation. When $z \geq 5$, the interface is saturated with butanol. As more butanol is added, it partitions into the aqueous phase. This results in an increase in the radius of the droplet. Therefore, the microemulsion is unable to solubilize large amounts of the aqueous phase. Thus, phase separation occurs at lower values of ω_o. This point (z=5) is called the maximum solubilization capacity (ω_o^{max}) for this microemulsion system.

Solubilization studies were also conducted for other straight and branched chain alcohols like 1-propanol, 1-pentanol, 1-hexanol, iso-butanol, tertiary pentanol, and iso-pentanol (figures 3.3 and 3.4). All alcohols show qualitatively similar results as 1-butanol. There exists a maximum solubilization capacity, ω_o^{max} for a certain composition of alcohol/CTAB for each microemulsion system.

All straight chain alcohols show a lower ω_o^{max} than 1-butanol as shown in figure 3.5. As chain length of alcohol increases up to 1-butanol (C_4) the curvature effect is dominant because 1-butanol partitions better at the interface than lower chain alcohols which are more soluble in the aqueous phase. Thus, microemulsions with 1-butanol as cosurfactant have a higher radius of spontaneous curvature. Higher chain alcohols are more soluble in the oil phase and also have a smaller radius of spontaneous curvature than 1-butanol. The branched chain alcohols fluidize the interface more than straight

chain alcohols leading to a higher attractive interaction between the aqueous droplets, which decreases the stability of the microemulsions thus decreasing the critical radius, R_c and leading to phase separation at lower volumes of ferric nitrate solution. Beyond this radius, a phase containing a very low density of aqueous droplets separates from the original microemulsion in order to decrease the total free energy of the system [84].

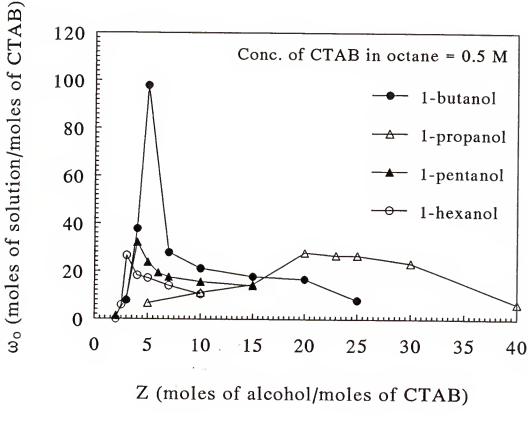

Figure 3.3 Effect of straight-chain alcohol cosurfactants on the solubilization of 0.05 M ferric nitrate solutions in microemulsions

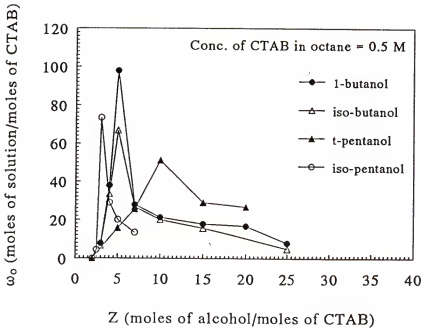

Figure 3.4 Effect of branched-chain alcohol cosurfactants on the solubilization of 0.05 M ferric nitrate solutions in microemulsions

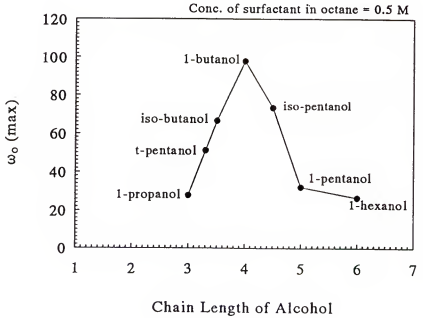

Figure 3.5 Maximum solubilization capacity of 0.05 M ferric nitrate solutions in microemulsions as a function of alcohol chain length

In the next experiment, the effect of oil chain length on the solubilization capacity of microemulsions for ferric nitrate was studied. 1-butanol was chosen as the co-surfactant for all these experiments. As the oil chain length increases, the solubility of CTAB decreases, thus decreasing the interfacial area and the radius of droplets. Increasing the oil chain length also increases the interaction between the droplets, which also lowers the solubilization capacity. This can be seen in figure 3.6 which shows maximum solubilization for microemulsions with heptane and octane, and a decrease in solubilization with increase in oil chain length.

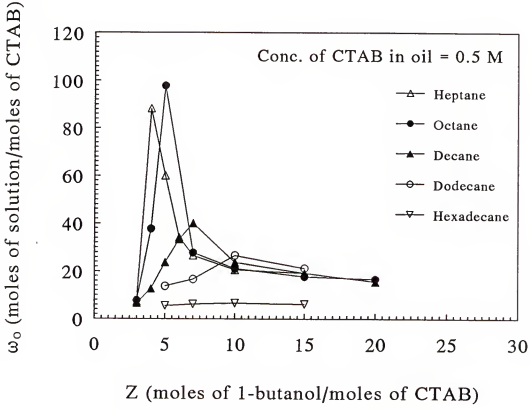

Figure 3.6 Effect of oil chain length on the solubilization of 0.05 M ferric nitrate solutions in microemulsions

Experiments were also performed for different surfactant chain lengths (C_{12}, C_{14} and C_{16}). The results clearly show (figure 3.7) that maximum solubilization is observed for the C_{16} surfactant (CTAB). The reason for this result is that CTAB partitions better at the interface as compared to the other two sufactants which are more soluble in the aqueous phase. Therefore, the radius of spontaneous curvature is higher for CTAB and it is able to solubilize larger amounts of ferric nitrate solution.

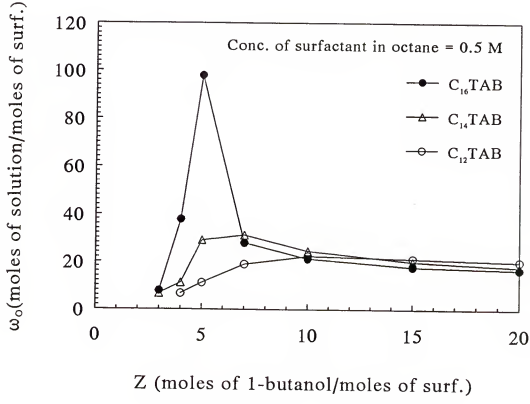

Figure 3.7 Effect of surfactant chain length on the solubilization of 0.05 M ferric nitrate solutions in microemulsions

From these experiments, it is evident that the microemulsion system which solubilizes the maximum amount of ferric nitrate solution should have CTAB as the surfactant, 1-butanol as the co-surfactant, and octane as the oil. The best composition was determined by varying the concentration of CTAB in octane and studying the solubilization capacity for ferric nitrate solutions. These results show (figure 3.8) that maximum solubilization occurs at a CTAB concentration in octane of 0.6 M.

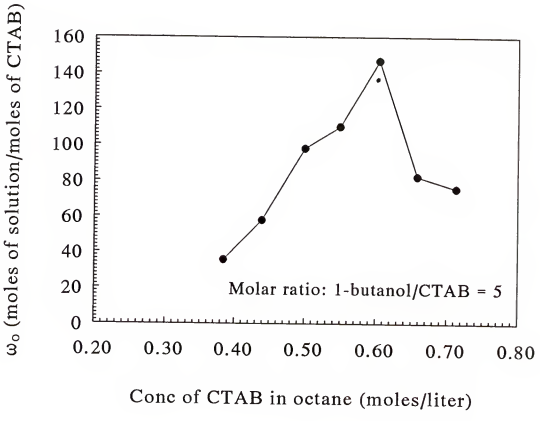

Figure 3.8 Effect of CTAB concentration on the solubilization of 0.05 M ferric nitrate solutions in microemulsions

Below this point (0.6 M), as surfactant concentration increases, it resides at the interface, thus increasing the radius of spontaneous curvature. Beyond this point, saturation of the interface is exceeded, and CTAB partitions into the oil phase. This increases the droplet interaction, thus decreasing the stability of the microemulsions and decreasing the critical radius of droplets.

On the basis of all these experiments, an optimum composition for a ferric nitrate solution/CTAB/1-butanol/octane microemulsion system was selected. This composition was used for the synthesis reactions described in the following chapter.

CHAPTER 4
SYNTHESIS OF IRON OXIDE USING MICROEMULSIONS

4.1 Introduction

Nanometer-sized magnetic particles are the subject of intense research because of their potential applications in high density magnetic recording and as constituents of magnetic fluids [53]. Since 1945, with the sudden growth in popularity of magnetic recording, γ-Fe_2O_3 in the form of small single domain particles has dominated the magnetic materials technology [56]. Besides their technological interest, iron oxide particles play an important role in the functioning of some biosystems [214]. It is well known that some bacteria use magnetic particles to navigate in the earth's magnetic field [215]. There is, however, lack of detailed data on the magnetic properties of well dispersed nanosize iron oxide particles, and on the behavior of these particles in relation to their synthesis conditions and size [216].

The first commercially available magnetic recording tapes produced in the late 1940s used iron oxide particles [217]. The most useful of the iron oxides is γ-Fe_2O_3, which still retains an important position in magnetic recording media, due to its great chemical and physical stability. Particle size and formation has greatly improved in the last four-and-a-half decades. The particles used in recording media today are acicular in shape. This shape anisotropy is the major contributor to the magnetic anisotropy,

with crystal anisotropy having a minor contribution. This gives rise to useful magnetic properties in terms of good coercivity and squareness ratio. The temperature dependence of magnetic properties for γ-Fe_2O_3 is very low [217,218].

Typical γ-Fe_2O_3 particles used for magnetic recording media are acicular with sizes in the order of 0.5 x 0.1 μm (l x d). These particles are non-porous so that they provide higher densities in the coating. γ-Fe_2O_3 currently used in recording media have typical coercivities of 300-400 Oe and saturation magnetization densities of about 350 emu/cm^3 of the coating. These properties, along with their great physical and chemical stability, make γ-Fe_2O_3 particles suitable for magnetic recording applications not requiring high recording densities [217,218].

γ-Fe_2O_3 has been synthesized by a variety of methods with the objective of producing uniform sized and ultrafine particles which can be used to produce dispersions for magnetic media. The usual method of preparation of γ-Fe_2O_3 is by reduction of α-Fe_2O_3 (synthesized from elongated α-FeOOH particles) to Fe_3O_4 and reoxidation to γ-Fe_2O_3 [56,218,219]. These particles have also been synthesized from iron (II) carboxylate by using iron (II) oxalate dihydrate [220-223]. Ozaki *et al.*[224] have used hydrothermal aging of aqueous solutions containing ferric ions in the presence of small amounts of phosphate ions. Nanosize particles of iron oxides have also been synthesized using an aerosol technique [225,226]. In most of these techniques, it is difficult to control the size distribution of the particles formed. This chapter describes the synthesis of γ-Fe_2O_3 nanoparticles using a microemulsion

mediated process wherein the nanosize aqueous droplets of water-in-oil microemulsions are used as constrained nano-reactors.

4.2 Synthesis of γ-Fe_2O_3

4.2.1 Experimental Procedure

4.2.1.1 Materials

Ferric nitrate and cobalt nitrate (> 99.99 % pure) were purchased from Aldrich. Ammonium Hydroxide solution (> 38 % NH_3); cetyl trimethyl ammonium bromide (CTAB) (technical grade); and n-butanol, methanol, and chloroform (all of HPLC grade) were purchased from Fisher Scientific. Octane (> 97% pure) was purchased from Phillips 66. All reagents were used without further purification. Water was deionized and distilled before use.

4.2.2.2 Methods

Based on the results of the solubilization experiments discussed in Chapter 3, a microemulsion system with CTAB as the surfactant, 1-butanol as the cosurfactant, n-octane as the oil phase and an aqueous solution as the water phase was chosen. This system was shown to solubilize a large amount of aqueous phase in well-defined nanosize droplets.

Microemulsions were prepared by solubilizing different salt solutions into CTAB/n-butanol/n-octane solutions. Two microemulsions (microemulsion I and microemulsion II) with identical compositions (see Table 4.1) but different aqueous phase were taken. This composition was obtained from the results of solubilization

experiments described in Chapter 3, specifically from the point near maximum solubilization in figure 3.8.

Table 4.1 Composition of the microemulsion systems used for the synthesis reactions

	Microemulsion I	Microemulsion II	Weight fractions
Aqueous Phase	0.05 M $Fe(NO_3)_3$	$(NH_4)OH$	0.41
Surfactant	CTAB	CTAB	0.11
Co-surfactant	n-butanol	n-butanol	0.10
Oil Phase	n-octane	n-octane	0.38

The aqueous phase in microemulsion I was a solution of ferric nitrate with a concentration of 0.05 M. The aqueous phase in microemulsion II was a solution of ammonium hydroxide, the precipitating agent, taken in a concentration 10% greater than that required stoichiometrically for complete precipitation of ferric hydroxide. These two microemulsions were then mixed under constant stirring. Due to the frequent collisions of the aqueous cores of water-in-oil microemulsions [90,132], the reacting species in microemulsions I and II come in contact with each other. This led to the precipitation of iron hydroxide particles within the nano-size aqueous droplets of the microemulsion. Since the two microemulsions (I and II) are of identical compositions,

differing only in the nature of the aqueous phase, the microemulsion does not get de-stabilized upon mixing. The aqueous droplets act as constrained nano-size reactors for the precipitation reaction, as the surfactant monolayer provides a barrier restricting the growth of the carbonate particles. This surfactant monolayer also hinders coagulation of particles. A schematic representation of this process is shown in figure 4.1.

The iron hydroxide precipitate synthesized in microemulsions was separated in a Sorvall RC-5B Superspeed Centrifuge at 7000 rpm for 10 minutes. The precipitate was then washed in a 1:1 mixture of methanol and chloroform, followed by pure methanol to remove any oil and surfactant from the particles. The precipitate was then dried at 100°C. Sintering of particles is not expected at this temperature.

Thermogravimetric analysis (TGA) was done on the dried powder in air with a heating rate of 5°C/min on a DuPont 900 Series TGA/DTA instrument. Differential thermal analysis (DTA) was done on the dried powder in air with a heating rate of 10°C/min. Based on the results of these analysis (discussed in the next section), the dried precipitate was heated (calcined) at 250°C for 5 hours to ensure conversion of the hydroxide particles into γ-Fe_2O_3.

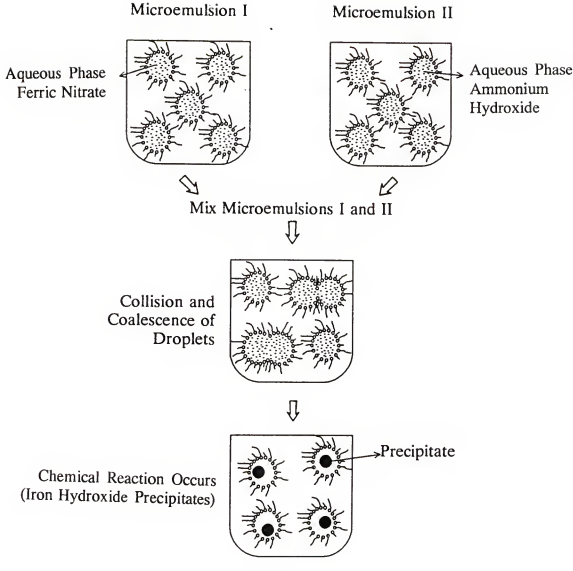

Figure 4.1 Schematic representation of synthesis of ferric hydroxide in microemulsions

Transmission electron microscopy (TEM) was used to study the size and size distribution of the precursor particles (hydroxides) as well as the calcined particles. In order to study the precursors, the washed precipitate was ultrasonically dispersed in methanol prior to depositing it onto a carbon coated TEM grid. TEM of the final product was done by ultrasonically dispersing the calcined powder in methanol prior to depositing it onto a carbon coated TEM grid. A JEOL 200CX transmission electron microscope was used for these studies.

Phase analysis of the calcined powder was done by powder X-ray diffraction on a Phillips PW1700 Powder Diffractometer at room temperature using Cu Kα radiation at 40 kV and 20 mA.

Magnetization (MH loop) measurements were done on an un-oriented, random assembly of particles at room temperature on a Vibrating Sample Magnetometer (LDJ 9600) with a maximum applied field of 1 kOe. The sample was prepared by hand pressing the calcined powder into a cylindrical pellet. No further heat treatments were done on the pellet.

4.2.2 Results and Discussion

Differential thermal analysis (DTA) of the precursor hydroxide powder showed three exothermic peaks at 225, 245 and 399°C (see figure 4.2). The first two peaks correspond to the conversion of the hydroxide into iron oxide and the crystallization of γ-Fe_2O_3. The third peak at 399°C corresponds to the formation of α-Fe_2O_3 which is non-magnetic. Therefore, calcination of precursors was done at 250°C.

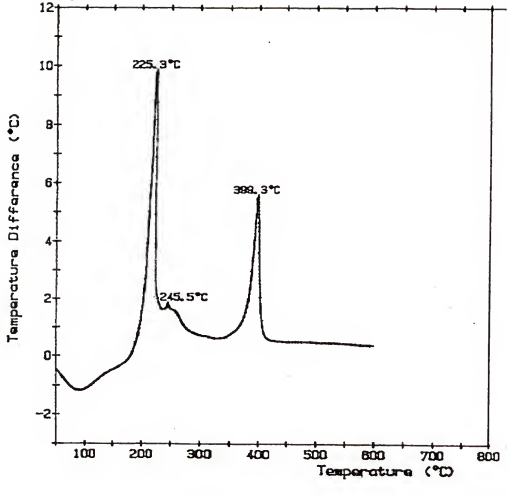

Figure 4.2 Differential thermal analysis of ferric hydroxide particles

The TEM micrograph (figure 4.3) of the precursor hydroxides show a range of particle size from 1 to 10 nm. These precursors are mainly spherical in structure, due to the spherical nature of the aqueous microdroplets in the microemulsions. By doing a simple calculation using the density of $Fe(OH)_3$ to be 3.4 gm/cm^3 and the diameter of microemulsion droplets to be 30 nm (experimentally determined by quasi-elastic light scattering), it was found that to form particles in this size range, the microemulsion droplets would have to collide and coalesce with exchange of material less than once

for a 1 nm particle and up to 20 times for a 10 nm particle. This assumes that each coalescence and exchange of material results in a complete reaction before the droplets break apart again. Therefore, the larger particles were formed by multiple collisions and coalescence. Since the aqueous reaction is very fast, it can be inferred that nucleation of the particle takes place upon the first coalescence followed by growth of particles in subsequent coalescences. The mechanism for the formation of very small nanoparticles (1 nm) can be explained as follows. Unreacted residual reactant in some of the droplets, upon coalescence with droplets containing the second reactant results in the formation of a precipitate with very small size (due to the small amount of the reactant).

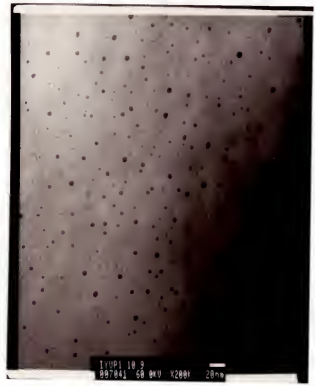

Figure 4.3 Transmission electron micrograph of precursor iron hydroxide particles

The TEM micrograph of calcined particles (figure 4.4) shows clusters of particles with sizes less than 10 nm. Due to the very small size of the particles and their agglomeration, it is very difficult to accurately determine the size or shape of these particles from this micrograph.

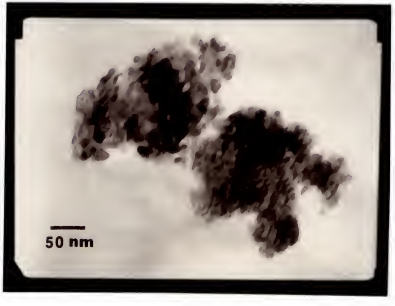

Figure 4.4 Transmission electron micrograph of γ-Fe_2O_3 particles

XRD pattern of the calcined sample shows that it contains γ-Fe_2O_3 as the majority phase with some α-Fe_2O_3 too present as an impurity (see figure 4.5). The ultrafine nature of these particles results in a broadening of peaks in the diffractogram. Since the peaks for both phases of iron oxide lie close to each other, it is not possible to determine the amount of the impurity phase in this sample.

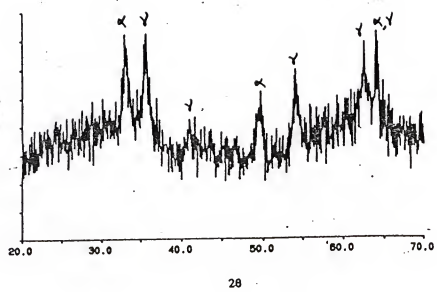

Figure 4.5 X-ray diffractogram of iron oxide particles

Magnetic measurements were done at room temperature on a VSM with a peak field of 1000 Oe. This yielded a saturation magnetization (M_s) of 18 emu/gm and an intrinsic coercivity of 62 Oe. γ-Fe_2O_3 has coercivities typically in the range of 300-400 Oe. These low values may be due to the presence of α-Fe_2O_3 which is non-magnetic or because some of the particles may be superparamagnetic.

The magnetic axis of a single particle is determined by the magnetic anisotropic energy of the particle. At low temperatures, in the absence of a magnetic field, the magnetic axis of single particles is randomly oriented. This leads to zero magnetization of sample. Under a sufficiently large magnetic field, all the magnetic axes are aligned,

giving rise to saturation magnetization. At sufficiently high temperatures, the magnetic anisotropy energy barrier of single domain particles is overcome by thermal energy, and superparamagnetism occurs wherein coercivity and remanent magnetization of particles becomes zero. With a decrease in particle size (down to nanometer size), thermal energy is large enough at room temperature to overcome the magnetic anisotropy energy leading to superparamagnetism at room temperature. This phenomenon would explain the low values for magnetic properties in iron oxide particles synthesized using microemulsions where the smaller particles may be superparamagnetic at room temperature.

4.3 Synthesis of Cobalt modified Iron Oxide

Iron oxides, due to their low coercivities, have a serious limitation for high density recording applications [217]. Coercivities of iron oxides can be raised to well above 1000 Oe, while retaining their practical benefits (like good chemical and physical stability) by modifying them with cobalt. Cobalt modified oxides particles are the predominant materials used in video tapes today, but they are also used in audio tapes and in some tapes and disks for high density digital recording. These uses make cobalt modified oxides the most commercially significant particulate recording material today [217,218].

Cobalt modification was initially done by uniformly doping iron oxides with Co^{2+} ions to form cubic or acicular particles. These were basically cobalt ferrite ($CoFe_2O_4$) particles and had coercivities greater than 1000 Oe. This enhancement in

coercivity takes place because the cobalt ions impart an increased magnetocrystalline anisotropy to the oxide structure (due to the coupling of the spins of the cobalt ions to the iron ions in the oxide structure). This results in particles with multi-axial anisotropy [217].

Cobalt-doped iron oxides are not completely suitable for magnetic recording applications due to a strong temperature dependence of coercivity and a high sensitivity to mechanical stress. To avoid these shortcomings, alternate methods have been recently used to enhance the coercivity of iron oxides. This was achieved by surface coating the iron oxide particles with cobalt, and it resulted in improved stability with respect to temperature and stress. There are two main methods for surface doping of iron oxides with cobalt. In the first method, iron oxide particles are suspended in an aqueous solution of Co^{2+} ions. A base (NH_4OH or NaOH) is added and the mixture is heated. This precipitates cobalt onto the surface of the particles. The temperature is not high enough to cause diffusion of cobalt to the core of the particle [217].

In the second method, γ-Fe_2O_3 particles are suspended in an aqueous solution of both Co^{2+} and Fe^{2+} ions in the ratio 1:2, and a base is added to this suspension and heated. A material close to the composition of $CoFe_2O_4$ precipitates on the surface of the particles. In both processes, the cobalt content is 3-6 percent by weight [217].

Cobalt modified iron oxides show uniaxial magnetic anisotropy, having a single preferred axis of magnetization like the oxide particles they are made from. The anisotropy due to cobalt reinforces that of the core particle due to the formation of a cobalt-rich surface. This uniaxial anisotropy and weak temperature dependence are both

lost if these surface-doped particles are annealed at high temperatures when cobalt diffuses into the interior of the particles [217,218].

The major thrust in cobalt-modified oxides these days is in the development of smaller size particles. This is to meet the increasing demands for high density recording applications for present and future video tapes. There are, however, practical limitations to how small these particles can be. Thermal considerations predict that cobalt-modified particles smaller than 10^{-16} cm^3 in volume will have coercivities that may change strongly with time. Other limitations include difficulty in manufacturing, and increased surface to volume ratio, meaning increased amounts of surfactant are required to disperse them [217].

Cobalt-modified iron oxides particles have been extremely successful in current recording applications and research is going on to improve their properties to meet future requirements. Typical commercially available cobalt surface modified iron oxide particles used in recording media have sizes of 0.3 x 0.05 μm, coercivity of 500 - 600 Oe and magnetization intensity of about 400 emu/cm^3 of coating.

Cobalt-doped iron oxide particles ($CoFe_2O_4$) have been synthesized by coprecipitating precursor hydroxides of Co^{2+} and Fe^{3+} in water-in-oil microemulsions. Cobalt-modified iron oxide particles (Co surface coated) have not been synthesized using microemulsions since it would be very difficult to control the uniformity of surface coating of cobalt on these particles in microemulsions.

4.3.1 Experimental Procedure

The microemulsion system chosen was the same as one described above except for the nature of the aqueous phase. The aqueous phase in one microemulsion contained cobalt (II) nitrate (0.01 M) and ferric nitrate (0.02 M) while the aqueous phase in the other microemulsion contained ammonium hydroxide (precipitating agent) in a quantity 10 % greater than that required stoichiometrically for complete precipitation of the hydroxide. The precipitate was separated, washed and dried as in the previous case to give cobalt-iron hydroxide nanoparticles. These particles were calcined at 600°C to ensure the complete conversion of the hydroxides into the magnetic ferrite ($CoFe_2O_4$).

4.3.2 Results and Discussion

X-ray diffraction of the calcined sample confirmed the formation of cobalt ferrite ($CoFe_2O_4$) with no impurities (see figure 4.6). TEM (figure 4.7) of the calcined particles showed agglomerates of particles less than 50 nm in size. This means that all particles are single domain in size since their sizes are less than the critical domain size for cobalt ferrite.

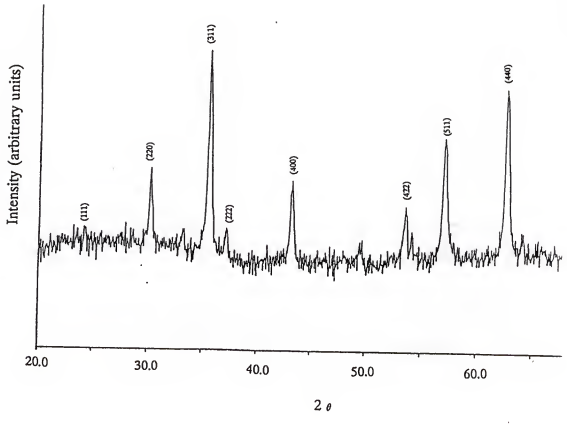

Figure 4.6 X-ray diffractogram of cobalt ferrite particles

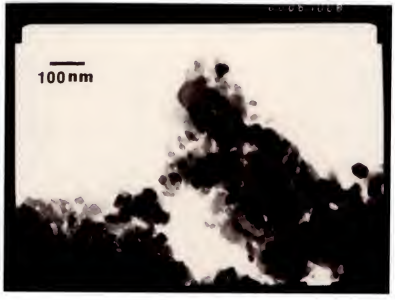

Figure 4.7 Transmission electron micrograph of cobalt ferrite particles

Magnetic measurements were done at room temperature on a VSM with a peak field of 10 kOe (see figure 4.8 for the MH loop). This yielded a saturation magnetization (M_s) of 65 emu/gm, a remanent magnetization (M_r) of 29 emu/gm and a coercivity of 1440 Oe which is higher compared to other values reported in literature for unoriented cobalt ferrite particles [217]. This indicates that the particles formed are single domain with no nonmagnetic impurities and that they are suitable for magnetic recording applications.

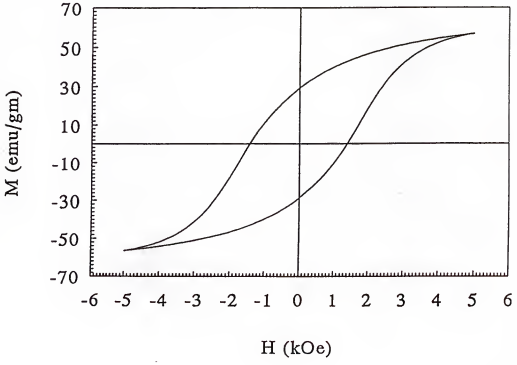

Figure 4.8 Magnetization loop for cobalt ferrite particles

4.4 Conclusions

In summary, γ-Fe_2O_3 nanoparticles have been synthesized using a microemulsion mediated process. These nanoparticles had low coercivity due to the presence of a non-magnetic phase and superparamagnetism in some particles due to their very small size. In order to improve these magnetic properties (see Table 4.2), iron oxide particles were doped with cobalt by coprecipitation in microemulsions.

Table 4.2 Comparison of magnetic properties for iron oxide and cobalt doped iron oxide nanoparticles

	Particle Size	H_c	M_s	M_r
Fe_2O_3	< 20 nm	62 Oe	18 emu/gm	~ 0
$CoFe_2O_4$	< 50 nm	1140 Oe	65 emu/gm	29 emu/gm

For the first time, cobalt doped iron oxide nanoparticles (cobalt ferrite) were synthesized using microemulsions. These particles had high coercivity (higher than previously reported in literature [217]) and high saturation magnetization, and are suitable for particulate magnetic recording applications.

CHAPTER 5
SYNTHESIS OF BARIUM FERRITE USING MICROEMULSIONS

5.1 Introduction

The hexagonal ferrite $BaFe_{12}O_{19}$ has been traditionally used in permanent magnets because of its high intrinsic coercivity and fairly large crystal anisotropy [227]. Until recently, these oxides had very little application in magnetic recording media. Pure barium ferrite has been used in many applications due to its high anisotropy (like in low-density recording on credit card strips) but its use in high-density magnetic recording was hindered by excessive particle size and very high coercivity [217]. Processes involving substitution of barium ferrite with Co and Ti, or Co and Sn have resulted in lower coercivities (~ 800 Oe) and plate like particles having diameter less than 0.1 μm. These particles, due to their shape and crystal anisotropy, have potential applications in perpendicular magnetic recording [228]. These flat platelets of barium ferrite, with their preferred axis perpendicular to their planes, can easily be oriented in a coating with its preferred axis of magnetization perpendicular to the surface.

Barium ferrite particles (pure and doped) have very good physical and chemical stability. Plate-like particles are now available in very small sizes with diameter up to 0.05 μm and plate thickness of about 0.01 μm. The magnetic properties of these particles are also satisfactory for magnetic recording. They have a narrow switching field distribution, probably due to the large magnetocrystalline anisotropy of barium

ferrite. Like other hexagonal ferrites, barium ferrite has a uniaxial magnetic anisotropy which is the sum of two effects, the crystalline anisotropy, and the shape anisotropy, which have opposite effects. This conflict of anisotropies, each with its own temperature coefficient, gives the coercivity of barium ferrite a more complicated temperature dependence compared to other magnetic oxides [217].

In the past few years, barium ferrite particles have undergone intensive development due to their potential in perpendicular magnetic recording. However, these particles have been rather slow to find commercial applications. Some current applications of barium ferrite particles include their use in high density flexible disks and digital audio tapes, but these applications are rather limited. The main limitation of barium ferrite with respect to advanced application is its relatively low magnetization intensity of about 300 emu/cm^3 of coating. This is less than that of most of the acicular oxides and considerably less than that of metallic particles. They are also costlier than the acicular oxides. Therefore, current research on barium ferrite focusses on the enhancement of the magnetization intensity, and control of the coercivity-temperature coefficients. Addition of dopants such as Sn and Zn have been found useful in this regard [217].

In the past decade, there has been an increasing interest in methods for the preparation of barium ferrite due to its emerging applications in perpendicular magnetic recording [228]. Such technological applications require materials with a strict control of homogeneity, particle size and shape, and magnetic characteristics.

The classical ceramic method for the preparation of barium ferrite consists of firing mixtures of iron oxide and barium carbonate at high temperatures (~1200°C) [229,230]. Furthermore, the ferrite must then be ground to reduce the particle size from multi domain to single domain. This generally yields mixtures which are non-homogeneous on a microscopic scale. Milling introduces lattice strains in the material, whereas high reaction temperatures induce sintering and coagulation of particles, both of which can be damaging if specific properties like uniform and reduced particle sizes, and high coercivities are required in the final product [231,232].

In order to achieve a homogeneity of ions on the atomic level and to overcome the effects of milling, various techniques such as chemical coprecipitation [233-235], glass crystallization [228,236], organometallic precursor method [237,238], aerosol synthesis [239,240], and colloidal synthesis [241] have been developed to prepare ultrafine barium ferrite. In this chapter, a water-in-oil microemulsion has been used as a reaction medium in order to produce uniform-sized, microhomogeneous nanoparticles of carbonate precursors for the synthesis of ultrafine barium ferrite.

5.2 Experimental Procedure

5.2.1 Materials

Barium chloride, ferric chloride, cobalt chloride and tin(IV) chloride (> 99.9% pure) were purchased from Aldrich Chemical Co. Ammonium carbonate (HPLC grade); CTAB (technical grade); and n-butanol, methanol, and chloroform (all of HPLC

grade) were purchased from Fisher. Octane (> 99% pure) was purchased from Sigma. All reagents were used without further purification. Water was deionized and distilled before use.

5.2.2 Methods

A microemulsion similar to one used for the synthesis of iron oxides was used for the synthesis of barium ferrite (see Table 5.1 for the compositions). This system solubilizes a relatively large volume of aqueous phase in well defined nano-size droplets of stable, single phase water-in-oil microemulsions.

Table 5.1 Composition of the microemulsion systems used for the synthesis reactions

	Microemulsion I	Microemulsion II	Weight fractions
Aqueous Phase	0.011 M $BaCl_2$ + 0.12 M $FeCl_3$	0.19 M $(NH_4)_2CO_3$	0.34
Surfactant	CTAB	CTAB	0.12
Co-surfactant	n-butanol	n-butanol	0.10
Oil Phase	n-octane	n-octane	0.44

Microemulsions were prepared by solubilizing different salt solutions into CTAB/n-butanol/n-octane solutions. We took two microemulsions (microemulsion I and microemulsion II) with identical compositions (see Table 5.1) but different aqueous phase. The aqueous phase in microemulsion I was a mixture of barium chloride and ferric chloride solutions in the molar ratio of 1.1:12. Even though, according to stoichiometry, a ratio of 1:12 should be sufficient, an excess of barium chloride was used because it is necessary for the precipitation of Ba^{2+} and Fe^{3+} ions in the ratio of 1:12 as barium carbonate is partially soluble in water. The aqueous phase in microemulsion II was the precipitating agent, ammonium carbonate, taken in a stoichiometric quantity required for complete precipitation of the cations. For the synthesis of cobalt and tin doped barium ferrite, salts of Co^{2+} and Sn^{4+} were substituted for Fe^{3+} in the aqueous phase of the first microemulsion in the form of chlorides. Different quantities of dopants were added to obtain $BaFe_{12-2x}Co_xSn_xO_{19}$ with x varying from 0.2 to 0.8.

These two microemulsions are then mixed under constant stirring. Due to the frequent collisions of the aqueous cores of water-in-oil microemulsions [90,132], the reacting species in microemulsions I and II come in contact with each other. This leads to the precipitation of barium-iron-carbonate within the nano-size aqueous droplets of the microemulsion. Since the two microemulsions (I and II) are of identical compositions, differing only in the nature of the aqueous phase, the microemulsion does not get de-stabilized upon mixing. The aqueous droplets act as constrained nano-size reactors for the precipitation reaction, as the surfactant monolayer provides a barrier

restricting the growth of the carbonate particles. This surfactant monolayer also hinders coagulation of particles. A schematic representation of this process is shown in figure 5.1.

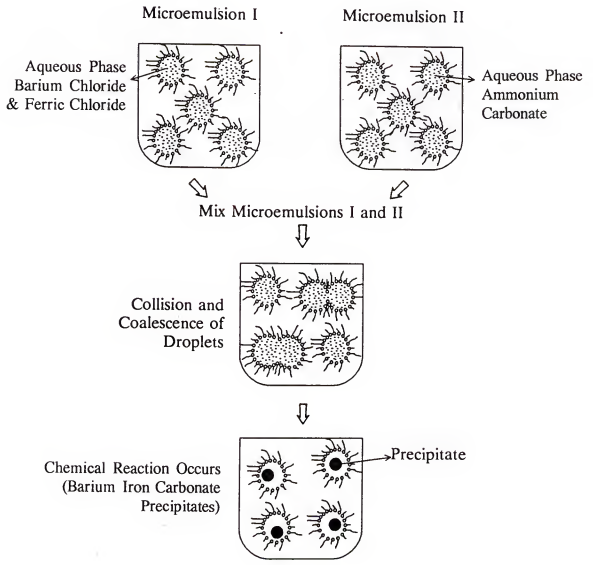

Figure 5.1 Schematic representation of synthesis of barium-iron carbonate precursors in microemulsions

The barium-iron-carbonate precipitate was separated in a Sorvall RC-5B Superspeed Centrifuge at 5000 rpm for 10 minutes. The precipitate was then washed in a 1:1 mixture of methanol and chloroform, followed by pure methanol to remove any oil and surfactant from the particles. The precipitate was then dried at 100°C. Sintering of particles is not expected at this temperature.

Thermogravimetric analysis (TGA) was done on the dried powder in air with a heating rate of 5°C/min on a DuPont 900 Series TGA/DTA instrument. Differential thermal analysis (DTA) was done on the dried powder in air with a heating rate of 10°C/min. Based on the results of these analysis (discussed in the next section), the dried precipitate was heated (calcined) at 950°C for 12 hours to ensure complete conversion of the carbonates into the hexaferrite ($BaFe_{12}O_{19}$).

Transmission electron microscopy (TEM) was used to study the size and size distribution of the precursor particles (carbonates) as well as the calcined particles. In order to study the precursors, the washed precipitate was ultrasonically dispersed in methanol prior to depositing it onto a carbon coated TEM grid. TEM of the final product was done by ultrasonically dispersing the calcined powder in methanol prior to depositing it onto a carbon coated TEM grid. A JEOL 200CX transmission electron microscope was used for these studies.

Phase analysis of the calcined powder was done by powder X-ray diffraction on a Phillips PW1700 Powder Diffractometer at room temperature using Cu Kα radiation at 40 kV and 20 mA.

Magnetization (MH loop) measurements were done on an un-oriented, random assembly of particles at room temperature on a Vibrating Sample Magnetometer (LDJ 9600) with a maximum applied field of 15 kOe. The sample was prepared by hand pressing the calcined powder into a cylindrical pellet. No further heat treatments were done on the pellet.

5.3 Results and Discussion

The transmission electron micrograph of the precursor carbonates (Figure 5.2) shows that the precursor particles formed within the aqueous droplets of the microemulsion are fairly monodispersed with a size range of 5-15 nm. By doing a simple calculation using the density of barium-iron carbonate to be 4.0 gm/cm^3 and the diameter of microemulsion droplets to be 30 nm (experimentally determined by quasi-elastic light scattering), it was found that the microemulsion droplets would have to collide and coalesce with exchange of material between 1 and 25 times to form particles in this size range. This assumes that each coalescence and exchange of material results in a complete reaction before the droplets break apart again.

Figure 5.2 Transmission electron micrograph of barium-iron carbonate particles

TEM of the calcined powder (Figure 5.3) shows barium ferrite particles in the size range of 50-100 nm, implying that growth of particles has taken place during calcination.

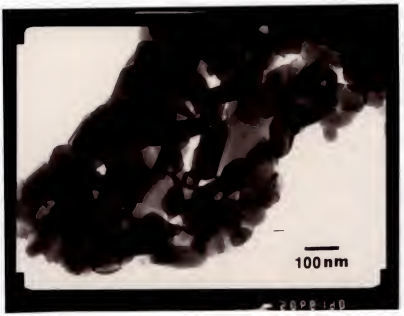

Figure 5.3 Transmission electron micrograph of barium ferrite particles

The TGA curve (Figure 5.4) shows three distinct weight loss steps. These steps are associated with the vaporization of water and organic moieties; and the conversion of ferric carbonate and barium carbonate into their respective oxides. It can also be seen from this graph that there is no weight change above 900°C, indicating the existence of only the oxide above this temperature.

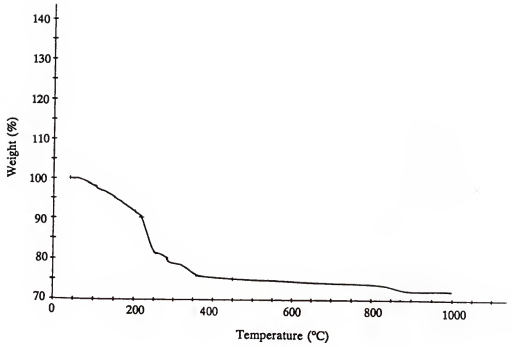

Figure 5.4 Thermogravimetric analysis of precursor particles

The DTA curve (Figure 5.5) shows an exothermic peak associated with the sharp weight loss in the TGA curve. A magnified view of this curve (see inset of Figure 5.5) shows that a small endotherm exists around 923°C implying that phase transformation to the hexaferrite occurs around this temperature. Therefore, calcination of the precursors was done at 950°C to ensure complete phase transformation.

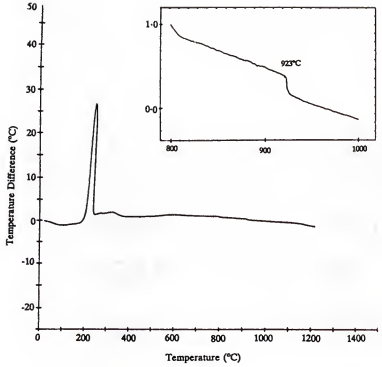

Figure 5.5 Differential thermal analysis of precursor particles

The XRD pattern for the calcined powder (Figure 5.6) shows all the characteristic peaks for barium ferrite marked by their indices. No other phases are detectable. This confirms the complete conversion of the precursor carbonates into the hexagonal ferrite $BaFe_{12}O_{19}$.

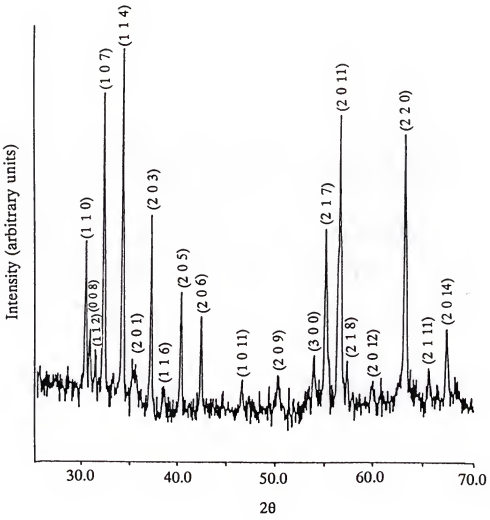

Figure 5.6 X-ray diffractogram for barium ferrite particles

The room temperature magnetization curve for the calcined powder, obtained on the VSM, is shown in Figure 5.7. The magnetic property measurements yielded an intrinsic coercivity (H_c) of 5397 Oe and a saturation magnetization (M_s) of 61.2 emu/gram (see Table 5.2 for a complete list of magnetic properties measured). This

high value of coercivity indicates that the barium ferrite particles formed by microemulsion processing are essentially single domain. This observation is also confirmed by the fact that the particles formed by us are in the size range of 50-100 nm. Haneda *et al.*[243] have shown that using the theory of Kittel [244], the critical domain size for barium ferrite particles is about 1 μm. Also, direct observation of the domain structure of barium ferrite particles at room temperature by Goto *et al.*[245] confirms that the critical domain size is indeed in the region of 1 μm.

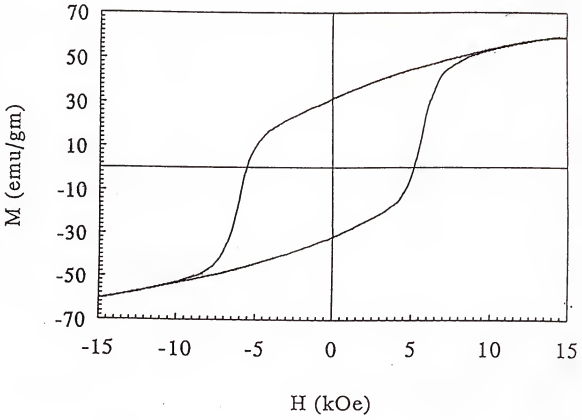

Figure 5.7 Magnetization loop for barium ferrite particles

However, the value of intrinsic coercivity, H_c obtained for our sample is lower than that theoretically calculated, $H_c \sim 6700$ Oe [246] using the model proposed by Stoner *et al.*[247] for an unoriented assembly of uniaxial single-domain particles in which magnetization reversal occurred through uniform rotation. The value of saturation magnetization, M_s is also lower than the saturation magnetization for single crystals of $BaFe_{12}O_{19}$, M_s of 72 emu/gram as reported by Shirk *et al.*[248]. Haneda *et al.*[234] have reported that reverse-domain nucleation greatly influences the intrinsic coercivity of precipitated powders. Reverse-domain nucleation may arise, even for stress-free chemically precipitated barium ferrite, at the edge of the particles. This may explain the discrepancy between experimental and theoretically calculated values of H_c and M_s for barium ferrite formed by microemulsion processing. Another reason may be poor crystallization of $BaFe_{12}O_{19}$ particles leading to amorphous impurities undetectable by X-ray diffraction.

Table 5.2 Magnetic Properties of microemulsion derived barium ferrite

Saturation Magnetization (M_s)	61.2 emu/gram
Intrinsic Coercivity (H_c)	5397 Oe
Remanent Magnetization (M_r)	33.3 emu/gram
Squareness Ratio (S_r)	0.54

In order to make these particles suitable for magnetic recording, the coercivity of barium ferrite has to be lowered to about 1000 to 1500 Oe. This can be done by doping these phase pure, single domain barium ferrite particles with Co and Sn [249]. Magnetization (MH loop) measurements were done at room temperature for doped barium ferrite ($BaFe_{12-2x}Co_xSn_xO_{19}$) synthesized using microemulsions with values of x = 0.2, 0.4, 0.6 and 0.8. Figure 5.8 shows the effect of doping on coercivity and saturation magnetization. TEM (figure 5.9) of these doped particles (for x=0.8) shows a size range of 50 to 100 nm (similar to pure barium ferrite).

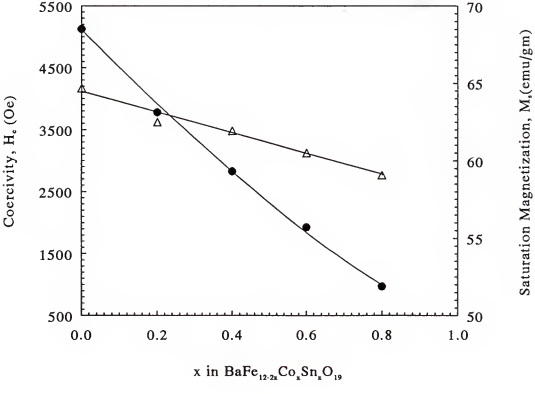

Figure 5.8 Effect of Sn and Co doping on coercivity and saturation magnetization of barium ferrite particles

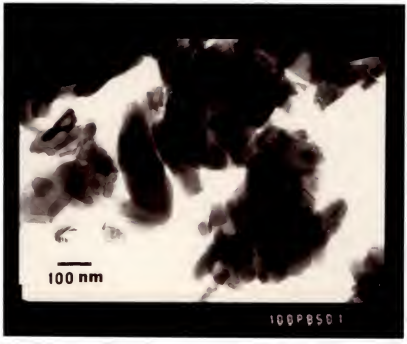

Figure 5.9 Transmission electron micrograph of $BaFe_{10.4}Co_{0.8}Sn_{0.8}O_{19}$

By using figure 5.8, we can prepare barium ferrite with a wide range of coercivities (with very little loss in magnetization) which will be suitable for magnetic recording.

5.4 Conclusions

In this chapter, a new process for the synthesis of ultrafine nanoparticles of barium ferrite using microemulsions has been described. These nanoparticles are essentially single domain with very high coercivity and saturation magnetization. These phase pure, single domain particles have also been doped by Co and Sn to reduce the coercivity and large anisotropy to make these particles suitable for high density perpendicular recording.

CHAPTER 6
REACTION KINETICS IN MICROEMULSIONS

6.1 Introduction

Over the past decade a concerted effort has been made to understand the structure, dynamics, and interactions of microemulsions [259,260], principally because of some applications and specially because the microemulsion droplet can be considered as a microreactor where certain chemical reactions take place within the very small domain provided by the droplet. Therefore, suitable control of the size of the droplet regulates the growth process for particle formation in microemulsions [48,49].

It has been reported by several authors [250-252] that in microemulsions, reaction rates and equilibria may be altered by several orders of magnitude as compared to reactions in homogeneous solutions. Therefore, much interest has been generated in microemulsions with respect to their unique properties as a reaction medium. In particular, research efforts have been devoted to the use of the aqueous droplets of water-in-oil microemulsions as a novel environment for enzyme catalyzed reactions [253,254] and the potential for selective synthesis [255,256], and the synthesis of nanoparticles (see Chapter 2).

The reaction rate and equilibria in microemulsions depend on the microemulsion composition, structure of various components of the microemulsion and the

hydrophobicity of the reactants [257]. The droplets in microemulsions are continuously diffusing through the continuous phase, leading to collisions between droplets. These collisions are inelastic and often called sticky collisions as they result in the coalescence of droplets and exchange of material between the droplets before they break apart [90,132]. For reaction in a water-in-oil microemulsion involving reactant species totally confined within the dispersed water droplets, a necessary step prior to their chemical reaction is transfer of reactants into the same droplet. When chemical reaction is fast (close to diffusion-controlled), the overall reaction rate is likely to be controlled by the rate of inter-droplet transfer of reacting species or "solubilizate exchange" [90]. Therefore, the nature of the collision process of droplets in microemulsions and the mechanism of transfer of reactants between two droplets (rate of coalescence of droplets) is of significance to the reaction kinetics. Fletcher *et al.*[261] have shown that for reactions on the nanosecond time scale (e.g. fluorescence measurements), droplets are essentially isolated, and no exchange occurs between droplets. For reactions in the microsecond to millisecond time scale, the inter-droplet exchange is the rate limiting step and the reaction rate depends on the reactant concentrations in the aqueous droplets. For reactions occurring in longer times, the inter-droplet exchange has no influence on the reaction rate [261].

Moya *et al.*[262] studied the oxidation of iodide ions by persulfate in water/ AOT/decane microemulsions. They reported reaction rates which followed second order kinetics and were higher than those for the same reaction in an aqueous solution.

The reaction rate decreases with an increase in water content but shows no dependence on surfactant concentration.

Lang *et al.*[263] have done a systematic study of the effect of oil, surfactant and cosurfactant alkyl chain length, and temperature on the rate constant for reactions involving exchange of material between colliding droplets in water-in-oil microemulsions. Their results were in agreement with current theories on the stability of microemulsions. They found that the rate constant increased with increase in temperature or oil chain length but rate constant decreased with increase in surfactant or cosurfactant chain length.

Fletcher *et al.*[90] have studied the exchange rates of aqueous solubilizates in AOT based water-in-oil microemulsions as a function of droplet size, temperature and oil chain length. Their results for electron transfer reactions indicated that these systems exhibited second order reaction kinetics. These reaction rates were two to four orders of magnitude slower than the droplet collision rate as predicted from simple diffusion theory. The reaction rate increased with increase in temperature and oil chain length, but decreased with increase in droplet size.

Similar studies have been described in this chapter, to understand this phenomenon for the microemulsion systems used for the synthesis of magnetic oxide nanoparticles by studying the effect of droplet size, aqueous concentration, cosurfactant and oil chain length.

An experimental method commonly used for the study of reaction kinetics in microemulsions is stopped-flow [90]. This method permits the fast mixing of two

reactants. The system derives its name from the fact that the flow of the sample is stopped immediately after mixing for monitoring the course of the reaction. The reactants to be mixed are placed in two syringes, the pistons of which are actuated by a pneumatic system. The reactants flow into a mixing chamber, where intimate mixing is achieved in 1 to 5 milliseconds, and then into an observation chamber, where the reaction is usually monitored by conductivity or optical detection (UV-Vis absorption or fluorescence) [258].

The objective of the experiments in this chapter was to study the reaction kinetics in the microemulsion systems used for the synthesis of iron oxide and barium ferrite nanoparticles and to study the effect of the chemical structure of various microemulsion components on the reaction rate. However, precipitation reactions cannot be directly studied using stopped-flow photometry since settling of particles and light scattering from particles would interfere with light absorbance measurements. Therefore, it is important to select reactants which do not precipitate while reacting, but can be monitored by light absorption or transmittance. Keeping this in mind, an electron transfer reaction between sodium hexachloroiridate(IV) and potassium ferrocyanide(II) was selected. Solutions of these two salts were used as aqueous phases in the two reactant microemulsions.

6.2 Experimental Procedure

6.2.1 Materials

Sodium hexachloroiridate(IV) (99.9 % pure) and potassium ferrocyanide(II) (99 % pure) were purchased from Aldrich. Cetyl trimethyl ammonium bromide (CTAB), 1-butanol, iso-butanol, 1-pentanol, iso-pentanol, 1-hexanol, 1-octanol, 1-decanol, n-hexane, n-octane, n-decane, n-dodecane, n-tetradecane (all technical grade) were purchased from Fisher Scientific. All reagents were used without further purification. Water was deionized and distilled before use. All experiments were carried out at room temperature.

6.2.2 Methods

A Perkin Elmer UV-Vis Spectrophotometer was used for absorbance measurements on three microemulsion systems. The first sample was a microemulsion with 0.5 mM sodium hexachloroiridate (SHCI) as the aqueous phase, 1-butanol as the cosurfactant, CTAB as the surfactant (0.5 M in octane), and octane as the oil phase. This microemulsion had a ω_o of 44.4 and a value of "z" equal to 5. The second sample was similar to the first microemulsion differing only in the nature of the aqueous phase which was a 0.5 mM solution of potassium ferrocyanide (PFC) in this case. The third sample was an equilibrium mixture of samples one and two, and has therefore been called the product microemulsion. All three samples were scanned for absorbance between wavelengths of 350 to 550 nm.

A Durrum-Dionex model D-110 Stopped-Flow Spectrophotometer was used to study the reaction kinetics in microemulsions. This instrument is a complete system for rapidly mixing two liquid reactant solutions and measuring their change in optical transmission or absorbance as a function of time. The reaction is observed by photometrically monitoring the transmission of light through a port in the mixing chamber cuvette. The output level sensed by the photometer is applied to an oscilloscope, where it is displayed against a time base. This data is then transferred to a personal computer through a GPIB port for data analysis. Monochromatic light is used in the photometer system so that each reaction can be studied at its optimum absorption peak. For these microemulsion systems, a wavelength of 490 nm was selected based on the UV-Vis absorbance measurements. All stopped-flow experiments were monitored by measuring the transmittance of light at this wavelength.

To study the effect of droplet size and aqueous phase concentration, samples were prepared by varying ω_o and aqueous phase concentration as required. Concentration of CTAB in oil was kept constant at 0.5 M and the molar ratio of cosurfactant to surfactant, z, was kept constant at 5.

For experiments on the effect of alcohol and oil chain length, the concentration of CTAB in oil was kept constant at 0.5 M. A required amount of aqueous phase was added to this mixture and then the cosurfactant (alcohol) was added drop by drop until the mixture became clear signifying the formation of the microemulsion phase. The compositions for all these systems are given in Table 6.1.

Table 6.1 Compositions of microemulsion systems used for studying effects of alcohol and oil chain length.

Alcohol	Oil	CTAB	ω_o
1-butanol (0.74 gm)	octane (5 ml)	0.9118 gm	22.2
1-pentanol (0.62 gm)	octane (5 ml)	0.9118 gm	22.2
1-hexanol (0.64 gm)	octane (5 ml)	0.9118 gm	22.2
1-octanol (0.64 gm)	octane (5 ml)	0.9118 gm	22.2
1-decanol (0.81 gm)	octane (5 ml)	0.9118 gm	22.2
iso-butanol (0.9 gm)	octane (5 ml)	0.9118 gm	22.2
iso-pentanol (0.7 gm)	octane (5 ml)	0.9118 gm	22.2
1-butanol (0.75 gm)	hexane (5 ml)	0.9118 gm	22.2
1-butanol (1.02 gm)	decane (5 ml)	0.9118 gm	22.2
1-butanol (0.64 gm)	dodecane (5 ml)	0.9558 gm	22.2

6.3 Results and Discussion

Figure 6.1 shows the results of UV-Vis absorbance measurements on the two reactant and one product microemulsion systems. The first reactant microemulsion containing sodium hexachloroiridate (SHCI) as the aqueous phase has two absorbance peaks at 425 nm and 490 nm. The second reactant microemulsion containing potassium

ferrocyanide has no absorbance peak in this range of wavelength. The product microemulsion had a very low absorption peak at 425 nm but no absorbance at 490 nm. The electron transfer reaction that has taken place in the aqueous phase of this microemulsion is as follows;

$$[IrCl_6]^{2-} + [Fe(CN)_6]^{4-} \rightarrow [IrCl_6]^{3-} + [Fe(CN)_6]^{3-}$$

It can be concluded from these results that the $[IrCl_6]^{2-}$ microemulsion system absorbs light at 425 and 490 nm, the product microemulsion system absorbs light at 425 nm, while the $[Fe(CN)_6]^{4-}$ microemulsion does not absorb light in this range. Since only one system (reactant microemulsion 1 - SHCI) has absorbance at 490 nm, this wavelength was selected to study these reactions in various microemulsion systems using stopped-flow photometry.

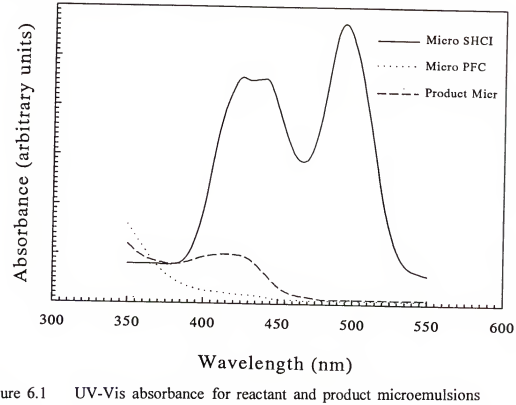

Figure 6.1 UV-Vis absorbance for reactant and product microemulsions

Figure 6.2 shows the raw data (transmittance of light at 490 nm vs time) for an aqueous phase/1-butanol/CTAB/n-octane microemulsion system. Initial intensity indicates that the previous sample which is present in the observation chamber. As the new sample enters the chamber, intensity suddenly decreases due to the high absorbance of light by microemulsion SHCI at 490 nm. Reaction begins at the point denoted t=0. As reaction proceeds, intensity of light increases as the reactant species $[IrCl_6]^{2-}$ is consumed, and products are formed. All results from this point onwards in this chapter will show only the part of the curve where reaction is taking place.

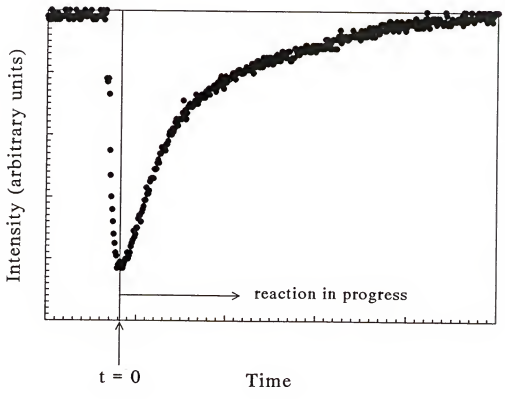

Figure 6.2 Raw data for stopped-flow photometry of reactions in microemulsions

Figure 6.3 is one such typical curve for the same microemulsion system as shown in figure 6.2. This figure shows the results for two experiments for the same sample, the curves for both experiments fall on each other, showing that these results are highly reproducible.

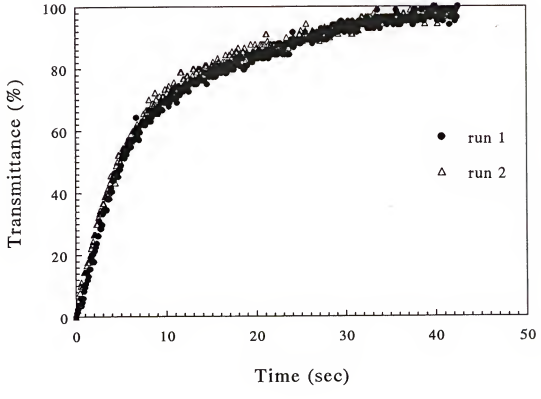

Figure 6.3 Reproducibility of data obtained for stopped-flow photometry of reactions in microemulsions

Experimental data for all reaction kinetics measurements were curve-fit to obtain the order of the reaction. These results gave orders ranging from 0.8 to 1.2 for all experiments. It can thus be inferred that all reactions in these microemulsion systems are close to first order. Also, since reactions controlled by diffusion and collision of droplets are expected to be second order, it can be said that the predominant factor controlling these reactions is the coalescence of droplets and not the collision rate between any two droplets.

The results for effect of droplet size in aqueous phase/1-butanol/CTAB/n-octane microemulsions are shown in figure 6.4. When the aqueous phase concentration was maintained at 0.5 mM (figure 6.4a), microemulsions with ω_o of 4.44 and 11.11 showed faster reaction rates than microemulsions with ω_o of 22.22 and 44.44. This result can be explained as follows. The droplets of all microemulsions have a bound layer of water (which cannot dissolve the reactant species) associated to the interface due to double layer formation [262]. At high ω_o values, the droplet size is large, therefore, there the volume of bound water is small compared to the free water in the solution. Therefore, the effective concentration of reactant will be lower in this case as compared to that in a small droplet where a majority of the water is in the form of bound water [262]. Since effective concentration is higher in smaller droplets, fewer collisions and coalescence between droplets will be required for the reaction to reach completion. Therefore, the reaction will be completed faster in these cases, as compared to a low effective concentration in the droplet. The following mathematical analysis can also be used to explain this point. The effective concentration of reactant can be expressed as

$$[A]_{eff} = n_A / V_w^f \qquad [6-1]$$

with

$$V_w = V_w^f + V_w^b \qquad [6-2]$$

where n_A is the number of moles of reactant, V_w is the total volume of water, V_w^f is the volume of free water, and V_w^b is the volume of bound water. Assuming that V_w^b is proportional to surfactant concentration [S], we can write

$$V_w^b = [S]\, d \qquad [6-3]$$

and therefore

$$[A]_{eff} = \frac{n_A}{V_w (1-d/\omega_o)} = \frac{[A]_{aq}}{1 - d/\omega_o} \qquad [6-4]$$

where $[A]_{aq}$ is the molar concentration of reactant in the aqueous solution and ω is the water content given by

$$\omega_o = \frac{V_w}{[S]} \qquad [6-5]$$

Therefore, the rate of the reaction can be expressed as

$$v = k\,[A]_{eff} = k \frac{[A]_{aq}}{1 - d/\omega_o} \qquad [6-6]$$

where k is the rate constant of the reaction. This expression clearly shows that as ω_o increases, the rate of the reaction goes down. However, at low aqueous phase concentrations, the effective concentration does not change appreciably with droplet size, therefore there is no change in reaction rate at low aqueous phase concentrations

(0.25 mM and 0.1 mM) as seen in figures 6.4b and 6.4c. This effect can also be seen in figures 6.5a and 6.5b where results for same droplet size, but different aqueous phase concentrations are plotted.

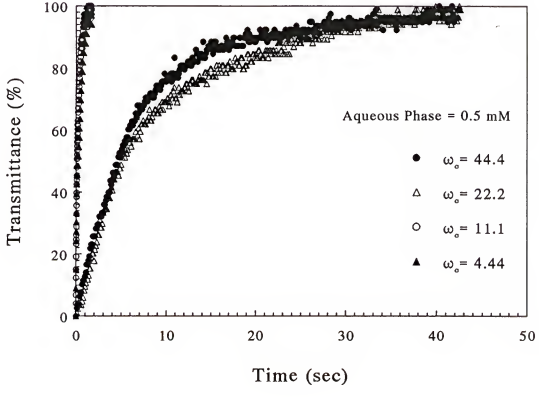

Figure 6.4 (a)

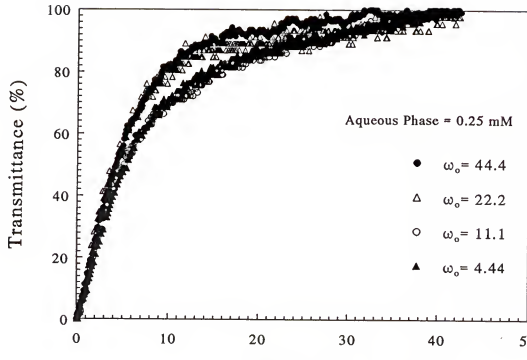

Figure 6.4 (b)

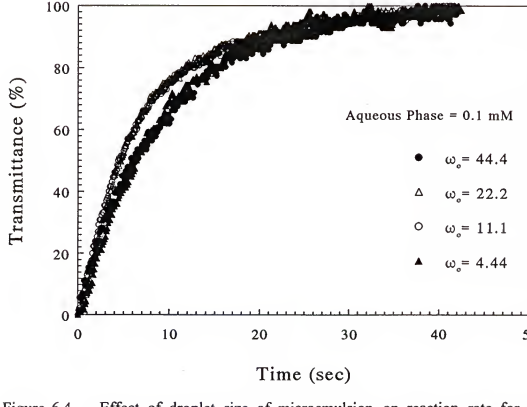

Figure 6.4 Effect of droplet size of microemulsion on reaction rate for aqueous phase concentrations of (a) 0.5 mM, (b) 0.25 mM, and (c) 0.1 mM

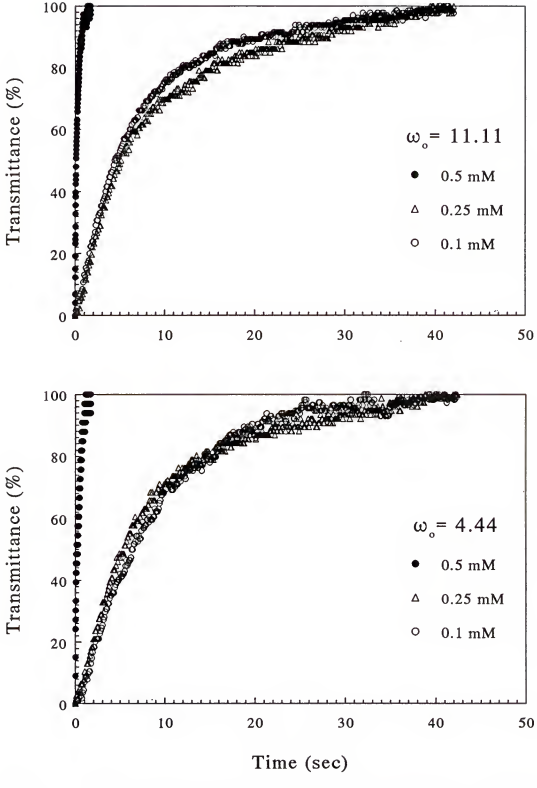

Figure 6.5 Effect of aqueous phase concentration on reaction rate in microemulsions for (a) ω_o = 11.11, and (b) ω_o = 4.44

Figure 6.6 shows the effect of alcohol chain length on the reaction rates in various microemulsion systems (compositions shown in Table 6.1). The reaction rates for microemulsions containing 1-butanol, 1-pentanol and 1-hexanol and similar to each other. Therefore, we can infer there is very little change in the fluidity of the microemulsion as the cosurfactant chain length is changed from 1-butanol to 1-hexanol. However, when 1-octanol is used as cosurfactant, the reaction rate decreases significantly. This can be attributed to the high rigidity of the interface for this system due to the chain length compatibility effect [264-266]. The chain length compatibility effect can be expressed as [266]

$$L_s = L_o + L_a \qquad [6-7]$$

where L_s is the carbon number of the surfactant, L_o is the carbon number of the oil, and L_a is the carbon number of the alcohol. Both 1-octanol and n-octane have 8 carbon atoms in their hydrophobic chain. The sum of these carbon atoms is exactly equal to the number of carbon atoms in the hydrophobic chain of CTAB which is sixteen. This chain length compatibility allows the chains to pack very well at the interface leading to a very rigid interface. A rigid interface slows down the reaction because it decreases the coalescence rate of the microemulsion droplets, fewer collisions of droplets result in coalescence. Lower coalescence rates means that reactants cannot come in contact with each other, thus slowing down the reaction. On the other hand, the microemulsion system having 1-decanol as the cosurfactant has a very fluid interface, and therefore a very high coalescence rate of microemulsion droplet and high rate of reaction.

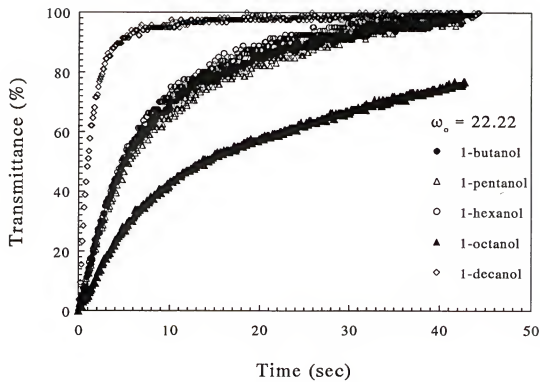

Figure 6.6 Effect of straight chain alcohols on rate of reaction in microemulsions

Figure 6.7 shows the effect of branched chain alcohol. It can be seen that there is very little change in reaction rates in these systems. Therefore, branched chain alcohol do not increase the fluidity of the interface significantly, and thus do not change the rate of the reaction very much.

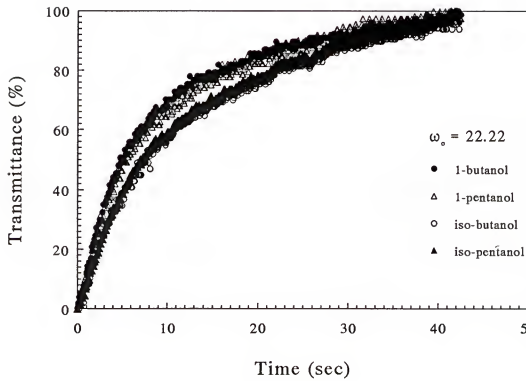

Figure 6.7 Effect of branched chain alcohols on rate of reaction in microemulsions

Results for the effect of oil chain length are shown in figure 6.8. A chain length compatibility effect can be seen in these results too for the microemulsion system with dodecane as oil phase [266]. Dodecane has 12 carbon atoms, 1-butanol has 4, giving a sum total of sixteen carbon atoms, which is exactly equal to that in CTAB. Therefore, systems containing dodecane as oil phase have a very high interfacial rigidity, and therefore a slower reaction rate.

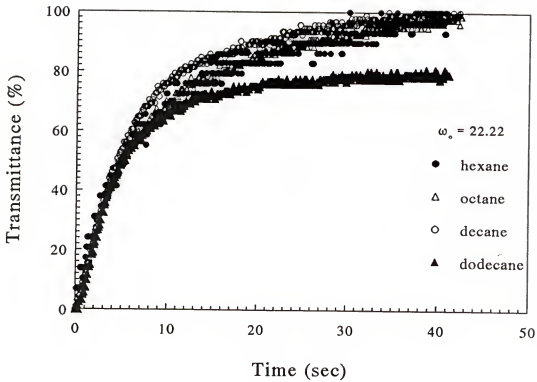

Figure 6.8 Effect of oil chain length on rate of reaction in microemulsions

6.4 Conclusions

In summary, in this chapter, reaction rates in microemulsion systems have been examined by studying the effect of several variables like, droplet size, aqueous phase concentration, cosurfactant chain length and oil chain length. Two main conclusions were reached on the basis of these results. First of all, as the droplet size in microemulsions decreases, the rate of the reaction increases. This has been explained

on the basis of an increase in the effective concentration of the aqueous phase in the droplets [262]. Secondly, chain length compatibility between the cosurfactant, oil and surfactant plays a significant role in determining the interfacial rigidity in microemulsions systems [264-266]. This rigidity causes the reaction rates in the aqueous phase/1-octanol/CTAB/octane and aqueous phase/1-butanol/dodecane/CTAB microemulsion systems to slow down significantly.

CHAPTER 7
CONCLUSIONS AND RECOMMENDATIONS FOR FUTURE WORK

7.1 Conclusions

In this dissertation, water-in-oil microemulsions have been used for the synthesis of magnetic oxide nanoparticles such as γ-Fe_2O_3, cobalt doped iron oxide ($CoFe_2O_4$), barium ferrite ($BaFe_{12}O_{19}$), and cobalt and tin doped barium ferrite. The aqueous cores of water-in-oil microemulsions were used as constrained, nanosize reactors for the precipitation of precursors which were less than 15 nm in size. These precursors were then heat treated to obtain the magnetic oxide. These particles were characterized by x-ray diffraction, transmission electron micrography and magnetic property measurements.

Chapter 3 described solubilization experiments used to characterize various microemulsion systems. These results were used to select a microemulsion suitable for the synthesis of nanoparticles, i.e., a system which solubilizes a large amount of aqueous phase. Such a system had CTAB as the surfactant, 1-butanol as the cosurfactant and octane as the oil phase.

Chapter 4 described the synthesis of γ-Fe_2O_3 and cobalt doped iron oxide ($CoFe_2O_4$) using a microemulsion system. The γ-Fe_2O_3 nanoparticles had a low coercivity and saturation magnetization due to the presence of α-Fe_2O_3 as an impurity

phase and due to superparamagnetism in some of the smaller particles. However, cobalt doped iron oxide ($CoFe_2O_4$) nanoparticles synthesized using microemulsions had high coercivity (higher than reported in literature) and high saturation magnetization, and were suitable for magnetic recording applications. This is the first report of the use of microemulsions for the synthesis of cobalt ferrite particles.

Chapter 5 described the synthesis of barium ferrite nanoparticles using microemulsions. These particles have very high coercivity and saturation magnetization. To make them suitable for magnetic recording applications, they were doped with cobalt and tin to reduce the coercivity. A curve was thus obtained to tailor barium ferrite particles of required coercivity without much loss in saturation magnetization. This is also the first time that microemulsions have been used for the synthesis of barium ferrite particles.

The effects for various components of the microemulsion on reaction rates were studied in Chapter 6. It can be inferred from the results that chain length compatibility plays a very important role in determining the interfacial rigidity in microemulsions. This controls the rate of the reaction, a fluid interface increases the rate while a rigid interface reduces the rate of the reaction. It can also be concluded that the droplet size of microemulsions has an effect on reaction rate as well. For high aqueous phase concentration, as the droplet size increases, the rate of the reaction decreases due to a decrease in the effective concentration of reactant in a droplet. This effect disappears at low aqueous phase concentrations.

7.2 Cost Analysis and Recycle

Although, there has been a lot of research on the synthesis of nanoparticles using microemulsions, there has been no effort to try to scale-up this process and make it commercially and economically viable. The main obstacle is the use of surfactants and several organic solvents in large quantities. If a method can be devised for the recycle and re-use of these components (as shown in figure 7.1), this technique could then be scaled-up for commercial purposes. After separation of particles by centrifugation, the supernatant can be separated into a mixture of oil, surfactant and cosurfactant, probably by distillation. These components can be used again to make new microemulsions. Solvents used for washing, such as methanol and chloroform can also be recycled after separation from the supernatant. A systematic study should be made to determine the percentage of all these chemicals that can be separated from the supernatant, and an economic analysis should be done before commercial use of this process is possible.

A preliminary cost analysis for the synthesis of barium ferrite using a aqueous phase/1-butanol/n-octane microemulsion system was done taking into account the cost of raw materials (chemicals) used. These prices are for high purity laboratory reagents, prices for chemicals purchased in larger quantities are expected to be much lower. For reactions in microemulsions, the product yield is usually of the order of 75 to 80 %, the rest of the product is lost during centrifugation and separation. Therefore, the cost analysis has been made for 75 % and 100 % yield, based on 0, 80, 90 and 100 % recycle of oil, surfactant and cosurfactant (see Table 7.1 for results). This analysis is

based on a typical laboratory scale reaction where about 0.5 gm of barium ferrite is produced.

Table 7.1 Cost analysis for the preparation of 1 gm of barium ferrite using microemulsions

	100 % yield	75 % yield
No recycle	$ 8.16 per gram	$ 10.88 per gram
80 % recycle	$ 2.05 per gram	$ 2.74 per gram
90 % recycle	$ 1.29 per gram	$ 1.72 per gram
100 % recycle	$ 0.53 per gram	$ 0.70 per gram

These results clearly show that the cost is reduced by a factor of four if 80 % of the organics are recycled. Therefore, recycling is an important aspect to be considered for scale-up and commercialization of this process.

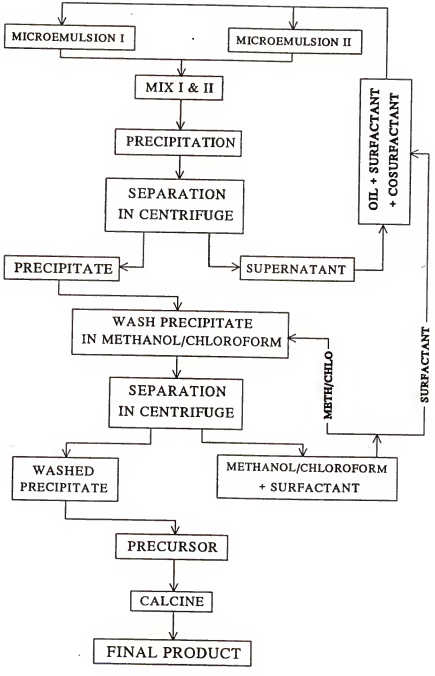

Figure 7.1 Recycling and re-use of organics for reaction in microemulsions

7.3 Recommendations for Future Work

From the present work, it is evident that further studies and experiments need to be performed in the following areas briefly described below.

For the synthesis of cobalt-modified iron oxide, surface doping of iron oxide nanoparticles with cobalt using microemulsions should be attempted. If successful, this would result in a better material for particulate magnetic recording [217] as well as demonstrate, for the first time, coating of particles in microemulsions.

Quasi-elastic light scattering (QELS) experiments on all microemulsion systems studied in this work should be done to measure the droplet interaction in these systems. This would be useful in explaining some of the results of solubilization experiments as well as the chain length compatibility effects in the reaction kinetics studies. QELS can also be used to measure droplet sizes in microemulsions before and after reactions. This may lead to development of methods to control and produce particles with narrower size distributions in microemulsions.

The interfacial compositions of microemulsion systems used for solubilization experiments (see Chapter 3) can be determined by Schulman-Bowcott plots of these systems for various values of z. This will give further insight to the solubilization phenomena.

Nanoparticles can be synthesized in various microemulsion systems by varying the alcohol and oil chain length to study the effect on particle size and shape, and magnetic properties. These results may be correlated to chain length compatibility effects seen in the reaction kinetics studies. It would also be interesting to study the

effect of calcination conditions (time and temperature) on the magnetic properties and size of barium ferrite nanoparticles synthesized using microemulsions.

In order to better understand the reaction mechanism in microemulsions, NMR and ESR studies can be used to study the rigidity or fluidity of interfaces in microemulsions. These results can then be correlated to stopped-flow reaction rate studies. Mathematical modelling of the complex dynamic processes in these systems should also provide a valuable insight into this phenomena.

REFERENCE LIST

1. Andres, R. P., Averback, R. S., Brown, W. L., Brus, L. E., Goddard III, W. A., Kaldor, A., Louie, S. G., Moscovits, M., Peercy, P. S., Riley, S. J., Siegel, R. W., Spaepen, F. and Wang, Y., J. Mater. Res., 4, 704 (1989).

2. Seigel, R. W., MRS Bulletin, 15, 60 (1990).

3. Han, Y. T., MRS Bulletin, 14, 13 (1989).

4. Jena, P., Rao, B. K. and Khanna, S. N., in Physics and Chemistry of Small Clusters, Plenum Press, New York (1987).

5. Brus, L. E., J. Phys. Chem., 90, 2555 (1986).

6. Gleiter, H., in Deformation of Polycrystals: Mechanisms and Microstructures, N. Hansen, A. Horsewell, T. Leffers, H. Lilholt, eds., Riso National Laboratory, Roskilde, Denmark, p. 15 (1981).

7. Birringer, R., Herr, U. and Gleiter, H., Suppl. Trans. Jpn. Inst. Met., 27, 43 (1986).

8. Siegel, R. W. and Hahn, H., in Current Trends in the Physics of Materials, M. Yussouff, ed., World Scientific Publ. Co. Singapore, p. 403 (1987).

9. Sugimoto, T., Adv. Coll. Interface Sci., 28, 65 (1987).

10. Uyeda, R., J. Cryst. Growth, 24, 69 (1974).

11. Liu, Y., Zhang, Q. L., Tittel, F. K., Curl, R. F. and Smalley, R. E., J. Chem. Phys., 85, 7434 (1986).

12. Morse, M. D., Chem. Rev., 86, 1049 (1986).

13. LaiHing, K., Wheeler, R. G., Wilson, W. L. and Duncan, M. A., J. Chem. Phys., 87, 3401 (1987).

14. Cannon, W. R., Danforth, S. C., Flint, J. H., Haggerty, J. S. and Marra, R. A., J. Amer. Ceram. Soc., 65, 324 (1982).

15. Rice, G. W. and Woodin, R. L., J. Amer. Ceram. Soc., 71, C181 (1988).

16. Rice, G. W. and Woodin, R. L., in Applications of Lasers to Industrial Chemistry, Proc. SPIE, 458 (1984).

17. Fayet, P. and Woste, L., Z. Phys. D, 3, 177 (1986).

18. Wright, R. B., Bates, J. K. and Gruen, D. M., Inorg. Chem., 17, 2275 (1978).

19. Leopold, D., Ho, J. and Lineberger, W. C., J. Chem. Phys., 86, 1715 (1987).

20. Zsigmondy, R., Z. Physik. Chem., 56, 6577 (1906).

21. Takiyama, K., Bull. Chem. Soc. Japan, 31, 944 (1958).

22. Turkevick, J., Stevenson, R. C. and Hillier J., Discuss. Faraday Soc., 11, 55 (1959).

23. Watillon, A. and Dauchot, J., J. Colloid. Inter. Sci., 27, 507 (1968).

24. Watillon, A. van Grunderbeeck, F. and Hautechler, M., Bull. Soc. Chim. Belges., 67, 5 (1958).

25. Sapieszko, R. S. and Matijevic, E., Corrosion, 36, 522 (1980).

26. Ottewill, R. H. and Woodbridge, R. F., J. Phot. Sci., 13, 98 (1965).

27. McFadyen, P. and Matijevic, E., J. Colloid. Inter. Sci., 44, 96 (1973).

28. Chiu, G. and Meehan, E. J., J. Colloid. Inter. Sci., 62, 1 (1977).

29. Joekes, I., Galembeck, F., Santos, H. S., Jafelicci, M., J. Colloid. Inter. Sci., 84, 278 (1981).

30. Matijevic, E., Langmuir, 2, 12 (1986).

31. Veale, C. R., in Fine Powders: Preparation, properties and uses, Halsted Press Division, Wiley & Sons, New York (1972).

32. Goldman, A. and Lang, A. M., J. Phys. Colloq., 297 (1987).

33. Kagawa, M., Kikuchi, M., Ohno, R. and Nagae. T., J. Amer. Ceram. Soc., 64, C-7 (1981).

34. LaMer, V. K. and Dinegar, R. H., J. Amer. Ceram. Soc., 72, 4847, (1950).

35. Ginell, R., Ginell, A. M. and Spoerri, P. E., J. Colloid. Inter. Sci., 2, 521 (1947).

36. Herak, M. J., Herak, M. M., Tezak, B. and Kratohvil, J., Arhiv. Kem., 27, 117 (1955).

37. Herak, M. J., Kratohvil, J., Herak and Wrischer, M. Croat. Chem. Acta, 30, 221 (1958).

38. Matijevic, E. and Wilhelmy, D. W., J. Colloid Inter. Sci., 86, 476 (1982).

39. Wilhelmy, D. W. and Matijevic, E., J. Chem. Soc., Farady Trans., 80, 563 (1984).

40. Wilhelmy, D. W. and Matijevic, E., Colloid Surf., 16, 1 (1985).

41. Brace, R. and Matijevic, E., J. Inorg. Nucl. Chem., 35, 3691 (1973).

42. Matijevic, E. and Scheiner, P., J. Colloid Inter. Sci., 63, 509 (1978).

43. Matijevic, E., Budnik, M. and Meites, L., J. Colloid Inter. Sci., 61, 302 (1977).

44. Berry, C. R., J. Opt. Soc. Am., 52, 888 (1961).

45. Berry, C. R., Marino, S. J. and Oster, C. F., Phot. Sci. Eng., 5, 332 (1961).

46. Berry, C. R. and Skillman, D. C., J. Opt. Soc. Am., 6, 159 (1962).

47. Robinson, B. H., Nature, 320, 309 (1986).

48. Boutonnet, M., Kizling, J., Stenius, P. and Maire, G., Colloids and Surfaces, 5, 209 (1982).

49. Lopez-Quintela, M. A. and Rivas, J., J. Colloid Interface Sci., 158, 446 (1993).

50. Hibst, H., J. Magn. Magn. Mater., 74, 193 (1988).

51. Bate, G., in Ferrites: Proc. ICF3, H. Watanabe, S. Iida and M. Sugimoto, eds., Center for Academic Publ., Japan, p. 509 (1981).

52. Imaoka, Y., Takada, K., Hamabata, T. and Murata, F., in Ferrites: Proc. ICF3, H. Watanabe, S. Iida and M. Sugimoto eds., Center for Academic Publ., Japan, 516 (1981).

53. Ozaki, M., MRS Bulletin, 12, 35 (1989).

54. Sharrock, M. P. and Bodnar, R. E., J. Appl. Phys., 57, 3919 (1985).

55. Mallinson, J. C., IEEE Trans. Magn., MAG-5, 182 (1969).

56. Craik, D. J., Magnetic Oxides, Parts 1 & 2, Wiley & Sons, New York (1975).

57. Roy, D. M., Nevrgaonkar, R. R., O'Holleran, T. P. and Roy, R., Bull. Amer. Ceram. Soc., 53, 421 (1974).

58. Nininger, R. C. and Schroeder, D., J. Phys. Chem. Solids, 39, 137 (1978).

59. Blesa, M. A. and Matijevic, E., Adv. Colloid. Inter. Sci., 29, 173 (1985).

60. Leung, R., Hou, M. J., Manohar, C., Shah D. O. and Chun, P. W., in Macro- and Microemulsions, D. O. Shah Ed., American Chemical Society, Washington D. C. (1985) p. 325.

61. Sharma, M. K. and Shah, D. O. in Macro- and Microemulsions, D. O. Shah Ed., American Chemical Society, Washington D. C. (1985) p. 1.

62. Hoar, T. P. and Schulman, J. H., Nature, 152, 102 (1943).

63. Schulman, J. H., Stoekenius, W. and Prince, L. M., J. Phys. Chem., 63, 1677 (1959).

64. Ostrovsky, M. V. and Good, R. J., J. Colloid Interface Sci., 102, 206 (1984).

65. Ruckenstein, E., in Surfactants in Solution, vol. 3, K. L. Mittal and B. Lindman Eds., Plenum, New York (1984) p. 1551.

66. Ruckenstein, E. and Chi, J. C., J. Chem. Soc. Faraday Trans. 2, 71, 1690 (1975).

67. Rosano, H. L. and Lyons, G. B., J. Phys. Chem., 89, 363 (1985).

68. De Gennes, P. G. and Taupin, C., J. Phys. Chem., 86, 2294 (1982).

69. Grimson, M. J. and Honary, F., Phys. Lett. A, 102, 241 (1984).

70. Safran, S. A., Turkevich, L. A. and Pincus, P., J. Phys. Lett., 45, 69 (1984).

71. Schulman, J. H. and Riley, D. P., J. Colloid Sci., 3, 383 (1948).

72. Marsden, S. S., in Surface Phenomena in Enhanced Oil Recovery, D. O. Shah Ed., Plenum, New York (1981) p. 151.

73. Schulman, J. H. and Friend, J. A., J. Colloid Interface Sci., 4, 497 (1949).

74. Graciaa, A., Lachaise, J., Chabrat, P., Letamendia, L., Rouch, J. and Vaucamps, C., J. Phys. Lett., 39, L235 (1978).

75. Bowcott, J. E. L. and Schulman, J. H., Z. Electrochem., 59, 283 (1955).

76. Miller, C. A., Hwan, R., Benton, J. and Fort, Jr., T., J. Colloid Interface Sci., 61, 547 (1977).

77. Bansal, V. K., Chinnaswamy, C., Ramachandran, C. and Shah, D. O., J. Colloid Interface Sci., 72, 524 (1979).

78. Gilberg, G., Lehtinen, H. and Friberg, S., J. Colloid Interface Sci., 33, 40 (1970).

79. Raey, J. C. and Buzier, M., in Surfactants in Solution, vol. 3, K. L. Mittal and B. Lindman Eds., Plenum, New York (1984) p. 1759.

80. Kaler, E. W., Bennet, K. E., Davis, H. T. and Scriven, L. E., J. Chem. Phys., 79, 5673 (1983).

81. Kaler, E. W., Davis, H. T. and Scriven, L. E., J. Chem. Phys., 79, 5685 (1983).

82. Cebula, D. J., Ottewill, R. H., Ralston, J. and Pusey, P. N., J. Chem. Soc., Faraday Trans., 77, 2585 (1981).

83. Dvolaitzky, M., Guyot, M., Lagues, M., Le Pesant, J. P., Ober, R., Sauterey, C. and Taupin, C., J. Chem. Phys., 69, 3279 (1978).

84. Hou, M. J. and Shah, D. O., Langmuir, 3, 1086 (1987).

85. Leung, R. and Shah, D. O., J. Colloid Interface Sci., 120, 320 and 330 (1987).

86. Hou, M. J., Kim, M. and Shah, D. O., J. Colloid Interface Sci., 123, 398 (1988).

87. Lang, J., Lalem, N. and Zana, R., Colloids and Surfaces, 68, 199 (1992).

88. Jada, A., Lang, J., Candau, S. J. and Zana, R., Colloids and Surfaces, 38, 251 (1989).

89. Fletcher, P. D. I. and Robinson, B. H., Ber. Bunsengs. Phys. Chem., 85, 857 (1981).

90. Fletcher, P. D. I., Howe, A. M. and Robinson, B. H., J. Chem. Soc. Faraday Trans. 1, 83, 985 (1987).

91. Jada, A., Lang, J., Zana, R., Makhloufi, R., Hirsch, E. and Candau, S. J., J. Phys. Chem., 94, 388 (1990).

92. Zana, R., Lang, J. and Canet, D., J. Phys. Chem., 95, 3364 (1991).

93. Luisi, P. L., Ang. Chemie, Int. Ed. Engl., 24, 439 (1985).

94. Cook. C. E. and Schulman, J. H., in Surface Chemistry, Munksgaurd, Copenhagen, p. 231 (1965).

95. Vinson, P. K., Bellare, J. R., Davis, H. T., Miller, W. G. and Scriven, L. E., J. Colloid Interface Sci., 142, 74 (1991).

96. Auvray, L., Cotton, J. P., Ober, R. and Taupin, C., J. Phys., 45, 913 (1984).

97. Scriven, L. E., Nature, 263, 123 (1976).

98. Tabony, J., Nature, 319, 400 (1986).

99. Dvolaitzsky, M., J. Phys. Chem., 84, 1532 (1980) and Meyer, C. T., Poggi, Y. and Maret G., J. de Physique, 43, 827 (1982).

100. Kon-no, K. and Kitahara, A., J. Colloid Interface Sci., 37, 169 (1971).

101. Eicke, H. F., J. Colloid Interface Sci., 68, 440 (1979).

102. Shinoda, K., Kuneida, H., Arai, T. and Saijo, H., J. Phys. Chem., 88, 5126 (1984).

103. Tamamusbi, B. and Watanabi, N., Colloid Polymer Sci., 258, 174 (1980).

104. Bansal, V. K., Shah, D. O. and O'Connell, J. P., J. Colloid Interface Sci., 75, 462 (1980).

105. Johnson, K. and Shah, D. O., J. Colloid Interface Sci., 107, 269 (1985).

106. Maitra, A., Vasta, G. and Eicke, H. F., J. Colloid Interface Sci., 93, 383 (1983).

107. Ruckenstein, E. and Krishnan, R., J. Colloid Interface Sci., 71, 321 (1979).

108. Mukherjee, S., Miller, C. A. and Fort, T., Jr., J. Colloid Interface Sci., 91, 223 (1983).

109. Jeng, J. F. and Miller, C. A., in Surfactants in Solution, vol.3, K. L. Mittal and B. Lindman, Eds., Plenum Press, New York, p.1829 (1984).

110. Huh, C., SPE / DOE, reprint 10728.

111. Jouffroy, J., Levinson, P. and De Gennes, P. G., J. Physique, 43, 1241 (1982).

112. Cazabat, A. M., Langevin, D., Meunier, J. and Pouchelon, A., Adv. Colloid Interface Sci., 16, 175 (1982).

113. Roux, D. and Bellocq, A. M., in Macro- and Microemulsions, D. O. Shah ed., Amer. Chem. Soc., Washington, DC, p. 105 (1985).

114. Huang, J. S. and Kim, M. W., Phys. Rev. Lett., 47, 1462 (1981).

115. Forche, G., Bellocq, A. M. and Brunetti, S., J. Colloid Interface Sci., 88, 302 (1982).

116. Safran, S. A. and Turkevich, L. A., Phys. Rev. Lett., 50, 1930 (1983).

117. Ayyub, P., Maitra, A. N. and Shah, D. O., Physica C, 168, 571 (1990).

118. Shah, D. O., Tamjeedi, A., Falcon, J. W. and Walker, Jr., R. W., AICHE J., 18, 1116 (1972).

119. Stoekenius, W., Schulman, J. H. and Prince, L. M., Kolloid-Z, 169, 170 (1960).

120. Schulman, J. H. and Montagne, J. B., Ann. N. Y. Acad. Sci., 92, 366 (1961).

121. Prince, L. M., J. Colloid Inter. Sci., 23, 165 (1967).

122. Miller, C. A. and Scriven, L. E., J. Colloid Inter. Sci., 23, 360 and 371 (1970).

123. Talmon, Y. and Prager, S., J. Chem. Phys., 69, 2984 (1978) and 76, 1535 (1982).

124. Widom, B., J. Chem. Phys., 81, 1030 (1984).

125. Gaines, G. L., in Insoluble Monolayers at Liquid-Gas Interfaces, Wiley, New York (1986).

126. Andelman, D., Cates, M. E., Roux, D. and Safran, S. E., J. Chem. Phys., 87, 7229 (1987).

127. Wheeler, J. C. and Widom, B., J. Amer. Che. Soc., 90, 3064 (1968).

128. Widom, B., J. Chem. Phys., 84, 6943 (1986).

129. Schick, M. and Shih, W. H., Phys. Rev. B., 34, 1797 (1986).

130. Chen, K., Ebner, C., Jayaprakash, C. and Pandit, R., J. Phys. C., 20, L361 (1987).

131. Eicke, H. F., Kubik, R., Hasse, R. and Zschokke, I., in Surfactants in Solution, vol. 3, Mittal, K. L. and Lindman, B. (Eds.), Plenum Press, New York, p. 1523 (1984).

132. Eicke, H. F., Shepherd, J. C. W. and Steinemann, A., J. Colloid Interface Sci., 56, 168 (1976).

133. Atik, S. S. and Thomas, J. K., J. Amer. Chem. Soc., 103, 3543 (1981).

134. Atik, S. S. and Thomas, J. K., Chem. Phys. Lett., 79, 351 (1981).

135. Fletcher, P. D. I., Howe, A. M., Perrins, N. M., Robinson, B. H., Toprakcioglu, C. and Dore, J. C., in Surfactants in Solution, vol. 3, Mittal, K. L. and Lindman, B. (Eds.), Plenum Press, New York, p. 1745 (1984).

136. Brochette, P. and Pileni, M. P., Nouv. J. Chim., 9, 551 (1985).

137. Lianos, P., Zana, R., Lang, J. and Cazabat, A. M., in Surfactants in Solution, vol. 6, Mittal, K. L. and Bothorel, P. (Eds.), Plenum Press, New York, p. 1365 (1986).

138. Howe, A. M., McDonald, J. A. and Robinson, B. H., J. Chem. Soc. Faraday Trans. 1, 83, 1007 (1987).

139. Corti, M. and Degiorgio, V., in Light Scattering in Liquids and Macromolecular Solutions, V. Degiorgio, M. Corti and V. Giglo, Eds., Plenum Press, New York, (1980).

140. Chang, N. J. and Kaler, E. W., Langmuir, 2, 184 (1986).

141. Cheng, D. C. and Gulari, E., J. Colloid Interface Sci., 90, 410 (182).

142. Calje, A. A., Agterot, W. and Vrij, A., in Micellization, Solubilization and Microemulsions, K. L. Mittal, Ed., Plenum Press, New York, p. 780 (1976).

143. Agterof, W. G. M., van Zomeren, J. A. J. and Vrij, A., Chem. Phys. Lett., 43, 363 (1976).

144. Cazabat, A. M., Langevin, D. and Pouchelon, A., J. Colloid Interface Sci., 73, 1 (1980).

145. Chew, C. H., Gan, L. M. and Shah, D. O., J. Disp. Sci. Tech., 11, 593 (1990).

146. Boutonnet, M., Kizling, J., Mintsa-Eya, V., Choplin, A., Touroude, R., Maire, G. and Stenius, P., J. Catalysis, 103, 95 (1987).

147. Touroude, R., Girard, P., Maire, G., Kizling, J., Boutonnet-Kizling, M. and Stenius, P., Colloids & Surfaces, 67, 19 (1992).

148. Clint, J. H., Collins, I. R., Williams, J. A., Robinson, B. H., Towey, T. F., Cajean, P. and Lodhi, A. K., Faraday Discuss., 95, 219 (1993).

149. Robinson, B. H., Khan-Lodhi, A. N. and Towey, T., in Structure and Reactivity in Reverse Micelles, M. P. Pileni ed., Elsevier, Amsterdam, p. 198 (1989).

150. Kurihara, K., Kizling, J., Stenius, P. and Fendler, J. H., J. Am. Chem. Soc., 105, 2574 (1983).

151. Wilcoxon, J. P. and Williamson, R. L., in Macromolecular Liquids, C. R. Safinaya, S. A. Safran and P. A. Pincus eds., Materials Research Society, Pittsburgh, p. 269 (1990).

152. Barnickel, P. and Wokaun, A., Mol. Phys., 69, 1 (1990).

153. Barnickel, P., Wokaun, A., Sager, W. and Eicke, H. F., J. Colloid Interface Sci., 148, 80 (1992).

154. Pileni, M. P. and Lisiecki, I., Colloids and Surfaces A: Physicochem. and Engg. Aspects, 80, 63 (1993).

155. Meyer, M., Wallberg, C., Kurihara, K. and Fendler, J. H., J. Chem. Soc., Chem. Commun., 90 (1984).

156. Lianos, P. and Thomas, J. K., Chem. Phys. Lett., 125, 299 (1986).

157. Petit, C. and Pileni, M. P., J. Phys. Chem., 92, 2282 (1988).

158. Modes, S. and Lianos, P., J. Phys. Chem., 93, 5854 (1989).

159. Petit, C., Lixon, P. and Pileni, M. P., J. Phys. Chem., 94 (1990) 1598.

160. Towey, T. F., Khan-Lodhi, A. N. and Robinson, B. H., J. Chem. Soc. Faraday Trans., 86, 3757 (1990).

161. Robinson, B. H., Towey, T. F., Zourab, S., Visser, A. J. W. G. and Van Hoek, A., Colloids and Surfaces, 61, 175 (1991).

162. Motte, L., Petit, C., Boulanger, L., Lixon, P. and Pileni, M. P., Langmuir, 8, 1049 (1992).

163. Tricot, Y. M., Rafaeloff, R., Emeren, A. and Fendler, J. H., in Organic Photo-transformations in Nonhomogeneous Media, M. A. Fox ed., ACS Symposium Series, The American Chemical Society, Washington, DC, 278, 99 (1985).

164. Dannhauser, T., O'Neil, M., Johansson, K., Whitten, D. and McLendon, G., J. Phys. Chem., 90, 6074 (1986).

165. Kortan, A. R., Hull, R., Opila, R. L., Bawendi, M. G., Steigerwald, M. L., Carroll, P. J. and Brus, L. E., J. Amer. Chem. Soc., 112, 1327 (1990).

166. Steigerwald, M. L., Alivisatos, A. P., Gibson, J. M., Harris, T. D., Kortan, R., Muller, R. J., Thayer, A. M., Duncan, T. M., Douglas, D. C. and Brus, L. E., J. Am. Chem. Soc., 110, 3046 (1988).

167. Kandori, K., Kon-no, K. and Kitahara, A., J. Colloid Interface Sci., 115, 579 (1987).

168. Kandori, K., Kon-no, K. and Kitahara, A., J. Colloid Interface Sci., 122, 78 (1988).

169. Roman, J. P., Hoornaert, P., Faure, D., Biver, C., Jacquet, F. and Martin, J. M., J. Colloid Interface Sci., 144, 324 (1991).

170. Kandori, K., Shizuka, N., Kon-no, K. and Kitahara, A., J. Disp. Sci. Tech., (1988).

171. Kon-no, K., Koide, M. and Kitahara, A., J. Chem. Soc. Japan, 6, 815 (1984).

172. Shizuka, N., Yanagi, M., Kon-no, K. and Kitahara, A., in Proceedings of the 37th Symposium on Colloid and Interface Chemistry, Morioka, Japan, p. 360 (1984).

173. Lumfimpadio, N., Nagy, J. B. and Derouane, E. G., in Surfactants in Solution, vol. 3, K. L. Mittal and B. Lindman Eds., Plenum, New York, p. 483, 1986.

174. Nagy, J. B., Colloids and Surfaces, 35, 201 (1989).

175. Yamauchi, H., Ishikawa, T. and Kondo, S., Colloids and Surfaces, 37, 71 (1989).

176. Osseo-Asare, K. and Arriagada, F. J., Colloids and Surfaces, 50, 321 (1990).

177. Arriagada, F. J. and Osseo-Asare, K., Colloids and Surfaces, 69, 105 (1992).

178. Wang, W., Fu. X., Tang, J. and Jiang, L., Colloids and Surfaces A: Physicochem. and Engg. Aspects, 81, 177 (1993).

179. Espiard, P., Mark, J. E. and Guyot, A., Polymer Bull., 24, 173 (1990).

180. Friberg, S. E. and Yang, C. C., in Innovations in Materials Processing Using Aqueous, Colloid and Surface Chemistry, F. M. Doyle, S. Raghavan, P. Somasundaran and G. W. Warren eds., The Minerals, Metals & Materials Society, Warrendale, p. 181 (1988).

181. Ward, A. J. I. and Friberg, S. E., MRS Bull., 41 (December 1989).

182. Guizard, C. et al., in Better Ceramics Through Chemistry III, C. J. Brinker, D. E. Clark and D. R. Ulrich eds., Mat. Res. Soc. Symp. Proc., Materials Research Society, Pittsburgh, 121, 115 (1988).

183. Watson, D. W., Fulton, J. L. and Smith, R. D., Materials Letters, 6, 31 (1987).

184. Boakye, E., Radovic, L. R. and Osseo-Asare, K., J. Colloid Interface Sci., 163, 120 (1994).

185. Bandow, S., Kimura, K., Kon-no, K. and Kitahara, A., Japanese J. Appl. Phys., 26, 713 (1987).

186. Lee, K. H., Sorensen, C. M., Klabunde, K. J. and Hadjipanayis, G. C., IEEE Trans. Magn., MAG-28, 3180 (1992).

187. Ayyub, P., Multani. M. S., Barma, M., Palkar, V. R. and Vijayaraghavan, R., J. Phys. C, 21, 2229 (1988).

188. Hou, M. J. and Shah, D. O., in Interfacial Phenomena in Bio-technology and Materials Processing, Y. A. Attia, B. M. Moudgil and S. Chander, Eds., Elsevier, Amsterdam, p. 443, 1988.

189. Kumar, P., Pillai, V., Bates, S. R. and Shah, D. O., Materials Letters, 16, 68 (1993).

190. Kumar, P., Pillai, V. and Shah, D. O., Appl. Phys. Lett., 62, 675 (1993).

191. Pillai, V., Kumar, P. and Shah, D. O., J. Magn. Mag. Mater., 116, L299 (1992).

192. Pillai, V., Kumar, P., Multani, M. S. and Shah, D. O., Colloids & Surfaces A: Physicochem. and Engg. Aspects, 80, 69 (1993).

193. Kumar, P., Pillai, V. and Shah, D. O., J. Magn. Mag. Mater., submitted.

194. Hingorani, S., Pillai, V., Kumar, P., Multani, M. S. and Shah, D. O., Mater. Res. Bull., 28, 1303 (1993).

195. Chabbra, V., Pillai, V., Mishra, B. K., Morrone, A. and Shah, D. O., Langmuir, in press (1995).

196. Leong, Y. S., Candau, F., Pouyet, G. and Candau, S., J. Colloid Interface Sci., 101, 167 (1984).

197. Ruckenstein, E., Chem. Phys. Lett., 57, 517 (1978).

198. Miller, C. A. and Neogi, P., AIChE J., 26, 217 (1980).

199. Huh, C., J. Colloid Interface Sci., 71, 408 (1979).

200. Miller, C. A., Hwan, R. W., Benton, W. J. and Fort, T., Jr., J. Colloid Interface Sci., 61, 554 (1977).

201. Cazabat, M., Langevin, D., Mennier, J., Abillon, O. and Chatenay, D., in Macro- and Microemulsions, D. O. Shah, ed., ACS, Washington, D.C., p. 75 (1980).

202. Eicke, H. F. and Rehak, J., Helv. Chim. Acta, 59, 2883 (1976).

203. Maitra, A., J. Phys. Chem., 88, 5122 (1984).

204. Mathews, M. B. and Hirschhorn, E., J. Colloid Interface Sci., 68, 22 (1979).

205. Nicholson, J. D. and Clark, J. H. R., in Surfactants in Solution, K. L. Mittal and B. Lindman, eds., Plenum, New York, p. 1663 (1984).

206. Adamson, A. W., J. Colloid Interface Sci., 29, 261 (1969).

207. Huh, C., J. Colloid Interface Sci., 97, 201 (1984).

208. Cazabat, A. M., Langevin, D. Meunier, J. and Pouchelon, A., J. Phys. Lett., 43, 89 (1982)

209. Chaternary, D., Abillon, O., Meunier, J., Langevin, D. and Cazabat, M., in Macro- and Microemulsions, D. O. Shah, ed., ACS, Washington, D. C., p. 119 (1985).

210. Safran, S. A., J. Chem. Phys., 78, 2073 (1983).

211. Helfrich, W., Z. Naturforsch., 28, 693 (1973).

212. Ruckenstein, E., J. Colloid Interface Sci., 114, 173 (1986).

213. Ayyub, P., Maitra, A. and Shah, D. O., J. Chem. Soc. Faraday Trans., 89, 3585 (1993).

214. Mann, S., Nature, 322, 119 (1989).

215. Blakemore, R., Science, 190, 377 (1975).

216. Vassiliou, J. K., Mehrotra, V., Russell, M. W. and Giannelis, E. P., Mat. Res. Soc. Symp. Proc., vol. 206, Materials Research Society, p. 561 (1991).

217. Sharrock, M. P., IEEE Trans. Magn., MAG-25, 4374 (1989).

218. Bate, G., in Magnetic Oxides, vol. 2, D. J. Craik, ed., Wiley Interscience, New York, p. 703 (1975).

219. Morrish, A. H., in Crystals: Growth and Applications, vol. 2, Springer, Berlin (1979).

220. Pesher, P. D. and Tsyrnorechki, O., Chem. Abstr., 55, 9137h (1961).

221. Tsyrnorechki, O. and Arshinar, I. V., Chem. Abstr., 55, 9138h (1961).

222. Rao, V., Shashimohan, A. L. and Biswas, A. B., J. Mater. Sci., 9, 430 (1974).

223. Seshan, K., Anantharaman, H. R., Rao, V., Shashimohan, A. L., Keer, H. V. and Chakravorty, D. K., Bull. Mater. Sci., 3a, 201 (1981).

224. Ozaki, M. and Matijevic, E., J. Colloid Interface Sci., 105, 99 (1985).

225. Tang, Z. X., Nafis, S., Sorensen, C. M., Hadjipanayis, G. C. and Klabunde, K. J., J. Magn. Mag. Mater., 80, 285 (1989).

226. Ramamurthi, M. and Leong, K. H., J. Aerosol Sci., 18, 175 (1987).

227. Cullity, B. D., in Introduction to Magnetic Materials, Addison-Wesley Publishing Company, Massachusetts, p. 575 (1972).

228. Kubo, O., Ido, T. and Yokoyama, H., IEEE Trans. Magn., MAG-18, 1122 (1982).

229. Kojima, H., in Ferromagnetic Materials, vol.3, E. P. Wohlfarth, ed., North-Holland, Amsterdam, p. 305 (1982).

230. Bye, G. C. and Howard, C. R., J. Appl. Chem. Biotechnol., 21, 319 (1971).

231. Haneda, K. and Kojima, H., J. Amer. Ceram. Soc., 57, 68 (1974).

232. Paulus, M., Preparative Methods in Solid State Chemistry, Academic Press, New York, p. 488 (1972).

233. Mee, C. D., and Jeschke, J. C., J. Appl. Phys., 34, 1271 (1963).

234. Haneda, K., Miyakama, C. and Kojima, H., J. Amer. Ceram. Soc., 57, 354 (1974).

235. Roos, W., J. Amer. Ceram. Soc., 63, 601 (1980).

236. Shirk, B. T. and Buessem, W. R., J. Amer. Ceram. Soc., 53, 192 (1970).

237. Licci, F. and Besagni, T., IEEE Trans. Magn., MAG-20, 1639 (1984).

238. Vallet, M., Rodriguez, P., Obradors, X., Isalgue, A., Rodriguez, J. and Pernet, M., J. de Physique, 46, C6-335 (1985).

239. Tang, Z. X., Nafis, S., Sorensen, C. M., Hadjipanayis, G. C., Klabunde, K. J., IEEE Trans. Magn., MAG-25, 4236 (1989).

240. Kaczmarek, W. A., Ninham, B. W. and Calka, A., J. Appl. Phys., 70, 5909 (1991).

241. Matijevic, E., J. Colloid Interface Sci., 117, 593 (1987).

242. Fendler, J. H., Chem. Rev., 87, 877 (1987).

243. Haneda, K. and Morrish, A. H., IEEE Trans. Magn., MAG-25, 2597 (1989).

244. Kittel, C., Rev. Mod. Phys., 40, 1294 (1969).

245. Goto, K., Ito, M. and Sakurai, T., Jap. J. Appl. Phys., 19, 541 (1980).

246. Haneda, K. and Kojima, H., J. Appl. Phys., 44, 3760 (1973).

247. Stoner, E. C. and Wohlfarth, E. W., Philos. Trans. Roy. Soc. London, Ser. A, 240, 599 (1948).

248. Shirk, B. T. and Buessem, W. R., J. Appl. Phys., 40, 1294 (1969).

249. Kubo, O., Ido, T. and Yokoyama, H., IEEE Trans. Magn., MAG-18, 1122 (1982).

250. Fendler, J. H., in Membrane Mimetic Chemistry, Wiley, New York (1982).

251. O'Connor, C. J., Lomax, T. D. and Ramage, R. E., Adv. Colloid Interface Sci., 20, 21 (1984).

252. Fletcher, P. D. I. and Robinson, B. H., J. Chem. Soc., Faraday Trans. I, 61, 1594 (1984).

253. Luisi, P. L., Angew Chem., 24, 7285 (1983).

254. Singh, C. P. and Shah, D. O., Colloids and Surfaces A: Physichochem. and Engg. Aspects, 77, 219 (1993).

255. Hilhorst, R., Laane, C. and Veeger, C., FEBS Lett., 159, 31 (1983).

256. Luthi, P. and Luisi, P. L., J. Amer. Chem. Soc., 106, 7285 (1984).

257. Minero, C., Pramauro, E. and Pelizzetti, E., Colloids and Surfaces, 35, 237 (1989).

258. Lang, J. and Zana, R. in Chemical Relaxation Methods, p. 405 (1990).

259. Lopez-Quintela, M. A. and Losada, D., Phys. Rev. Lett., 63, 1131 (1988).

260. Robinson, B. H., Chem. Br., 26, 342 (1990).

261. Fletcher, P. D. I. and Robinson, B. H., Ber. Bunsenges. Phys. Chem., 85, 863 (1981).

262. Moya, M. L., Izquierdo, C. and Casado, J., J. Phys. Chem., 95, 6001 (1991).

263. Lang, J., Lalem, N. and Zana, R., Colloids and Surfaces, 68, 199 (1992).

264. Shah, D. O. and Shiao, S. Y., Adv. Chem. Ser., 144, 153 (1975).

265. Sharma, M. K., Shiao, S. Y., Bansal, V. K. and Shah, D. O., in Macro- and Microemulsions, D. O. Shah ed., Amer. Chem. Soc., Washington, DC, p. 87 (1985).

266. Chattopadhyay, A. K., Shah, D. O. and Ghaicha, L., Langmuir, 8, 27 (1992).

BIOGRAPHICAL SKETCH

Vinod Kumar Pillai was born on January 13, 1968, in the state of Kerala in India. He received his B.Tech. degree in chemical engineering from the Indian Institute of Technology, Delhi, India in May, 1990. Subsequently, he joined the University of Florida, where he received his Ph.D. in chemical engineering in August, 1995.

I certify that I have read this study and that in my opinion it conforms to acceptable standards of scholarly presentation and is fully adequate, in scope and quality, as a dissertation for the degree of Doctor of Philosophy.

Dinesh O. Shah, Chairman
Professor of Chemical
Engineering

I certify that I have read this study and that in my opinion it conforms to acceptable standards of scholarly presentation and is fully adequate, in scope and quality, as a dissertation for the degree of Doctor of Philosophy.

Ranganatha Narayanan
Professor of Chemical
Engineering

I certify that I have read this study and that in my opinion it conforms to acceptable standards of scholarly presentation and is fully adequate, in scope and quality, as a dissertation for the degree of Doctor of Philosophy.

Gerald B. Westermann-Clark
Associate Professor of
Chemical Engineering

I certify that I have read this study and that in my opinion it conforms to acceptable standards of scholarly presentation and is fully adequate, in scope and quality, as a dissertation for the degree of Doctor of Philosophy.

Chang-Won Park
Associate Professor of
Chemical Engineering

I certify that I have read this study and that in my opinion it conforms to acceptable standards of scholarly presentation and is fully adequate, in scope and quality, as a dissertation for the degree of Doctor of Philosophy.

Brij M. Moudgil
Professor of Materials
Science and Engineering

This dissertation was submitted to the Graduate Faculty of the College of Engineering and to the Graduate School and was accepted as partial fulfillment of the requirements for the degree of Doctor of Philosophy.

August, 1995

Winfred M. Phillips
Dean, College of
Engineering

Karen A. Holbrook
Dean, Graduate School